
# Micro deformation Study on Insect's Wings using High Speed Digital Holographic Interferometry

Presented by

**Daniel Donato Aguayo, M. Sc.**

A Doctoral Thesis submitted in partial fulfilment of the requirements for award of Doctor of Philosophy of the Centro de Investigaciones en Optica A.C.

**May 2012**

**Thesis Director:**

**Dr. Fernando Mendoza Santoyo**

**Thesis Supervisor:**

**Dr. Manuel H. De la Torre Ibarra**


# Micro deformation Study on Insect's Wings using High Speed Digital Holographic Interferometry

Presented by

**Daniel Donato Aguayo, M. Sc.**

A Doctoral Thesis submitted in partial fulfilment of the requirements for award of Doctor of Philosophy of the Centro de Investigaciones en Optica A.C.

**May 2012**

**Thesis Director:**

**Dr. Fernando Mendoza Santoyo**

**Thesis Supervisor:**

**Dr. Manuel H. De la Torre Ibarra**

## Abstract

The research work presented in this thesis shows a successful and promising application of an optical non destructive testing technique known as Digital Holographic Interferometry (DHI). DHI is applied to detect and obtain deformations from butterflies' wings during flapping motion; this generates displacement maps for the whole wings surface.

The in-vivo tests and their corresponding results were recorded for five different winged butterfly species. The first part of this research work, presents the measurement performed on wings from a *Pterourus Multicaudata* known as Eastern Swallow Tiger Butterfly, as a proof of principle that fast non repeatable events on organic tissues can be detected with high accuracy using DHI. The second part of this work presents a comparison from four different specimens, namely *Nymphalis Antiopa* known as Mourning Cloak, *Agraulis Vanillae Incarnata* known as Gulf fritillary, *Danaus Gilippus Cramer* and *Precis Evarete Felder* known as Queen Butterfly and Buckeye Butterfly respectively. All of them have a different structure and wing shape.

The DHI optical set up used has an out of plane sensibility that enables to measure changes perpendicular to the wings surface with hundreds of nanometers resolution. The wings motion is recorded with a high speed camera at rates of 500 frames per second for the proof of principle test, and 4000 frames per second for the remaining tests. The camera uses CMOS technology with 800 x 800 pixels resolution and dynamic range of 10 bits; features that allow the detection of small changes during wings flapping.

The wing deformation maps are presented in a pseudo 3D representation, and they show the relative deformation of the insect's wing for a fraction of time during the up and down stroke movements. A time vs. displacement tracking plot of randomly chosen wing sections is presented to show the differences of behaviour among different wing sections of a butterfly during normal flapping**.**


**This is to certify that the work submitted in this thesis is original and that neither this thesis nor the original work contained here has been submitted to this or any other institution for a higher degree.**

| | |
|---|---|
| **Dr. Fernando Mendoza Santoyo** | **Dr. Manuel H. De La Torre Ibarra** |
| **Thesis Director** | **Thesis Supervisor** |

**“So here it is, another chance, wide awake, you face the day**

**Your dream is over...Or has it just begun?”**

Chris De Garmo

**“Realized I can never win, sometimes feel like I have failed**

**Inside where do I begin? My mind is laughing at me**

**Tell me, why am I to blame? Aren't we supposed to be the same?**

**That's why I will never tame this thing that’s burning in me?”**

J. Davis

Before you come to any conclusions, live by your own mistakes and stand by them...

Look inside the mirror, but I don't know who I see
Smoke another cigarette, a smile holds back the tears
These contradictions, seem to be the story of my life
A simple man with memories, of those long lost golden days
I close my eyes and slowly driftaway

Mistakes I've made remind me, of the roads I shouldn't choose
It never comes that easy, when you've nothing left to lose
I can't see the answers, tell me why am I so blind
A tired man, I'll make the best, of another lonely day
I close my eyes and slowly driftaway

Never thought I'd make it, Just from playing my guitar
Just a little smile, always shelters me from pain
Every time I start to slide,
I wish upon a star (no matter where we are)
The sun comes out, And dries up all the rain

I'm an honest man, who refused the shade
On a hot and lonely day,
I close my eyes and dream my life away
Now I know that I can stop the rain
Close my eyes and slowly driftaway
I Close my eyes and dream my life away

And you know I'm a dreamer, but my heart's of gold
I had to run away high, so, I wouldn't come home low
Just when things went right, it doesn't mean they were always wrong
Just take this song and you'll never be left all alone
Take me to your heart; Feel me in your bones
Just one more night, and I'm coming off this long & winding road

You know that I've seen, to many romantic dreams
Up in lights, falling off the silver screen
My heart's like an open book for the whole world to read
Sometimes nothing-keeps me together at the seams

I'm on my way; well I'm on my way
Home sweet home, tonight, tonight
I'm on my way, just set me free,
Home sweet home

**Nikki Sixx**

# Dedicatory

To my mother

# Concepción Aguayo Palomino

Not a single thing of this would be possible without You

Your love, understanding and support, I Love You!!

Even if I write on every single line in this page

Not a single word would express my love and appreciation to You

I know never will be enough but…

# Thank You, MOM!!!

To

# Fabiola León Galvan

Thanks for old and new memories and all the laughing,

For all the things lived with you after all those lost years,

I appreciate what you have done for me, being a true friend and

For keeping encouraging me to finish this last part of this process

I love the fact that you are my partner in crime and

For all of these, and too many other things…

# Thank You, Faby!

## Acknowledgments

I would like to express all my gratitude to my supervisor Dr. Fernando Mendoza Santoyo, who supports me through all this long and winding road that take my doctoral research work at CIO, and for his enormous patience and also for sharing his knowledge and experience. Thank you for all the support during my stay at Loughborough University.

I would like to express my gratitude to Manuel de la Torre and his family for all their support in many different ways and times, also I want to thank Manuel for sharing his time and knowledge, patience and support, and you know what I'm talking about, thank you my dear friend none of this would have been possible without your help, my total appreciation and gratitude to you. Thank for being a true friend in the hardest moments.

Also I would like to thank to Dr. Carlos Perez for sharing his time to be part of the examiners committee and for all the suggestions shared, in the same way I express my gratitude to Dr. Tonatiuh Saucedo for taking the time to participate as my external examiner and taking the time to review my work despite all his duties, to both of them thank you.

I want to thank to all my family, my parents, brother and sisters, and to all my nieces and nephews for their support in the darkest hours and all the ups and downs of this journey, for all the things they know thank you.

Thanks to Dr. Ramón Rodriguez Vera for his friendship and support in different moments of this adventure; to Efraín Mejía for all the talks and fun shared through all these years and to Dr. Manuel Salas Araiza for sharing his knowledge in the entomology field which was really helpful to finish this work.

I would like to express my gratitude to all my teachers at CIO, those who teach, share their knowledge and of course to all who share their time despite all of their duties, to all of them thank you. Also I want to thank to Dr. Jonathan M. Huntley and Dr. Pablo Ruiz for his patient and support during my stay at Loughborough University.

I would like to thank to all personnel at CIO in the whole different areas, who help me and support me in many different ways. Thanks Laura Gonzalez, Guillermina Muñiz, Angeles Sanchez, and the entire academic department who help me at any time and their assistance help me through the long way to the top (at this point). Also thanks to Mario Ruiz for all the help and his friendship.

I would also like to thank to all my friends in the CIO, no matter if we don't share enough time as we usually did in the past, I'll never forget your support, a special mention to my classmates Claudio Ramirez and Cornelio Alvarez for teaching me lots of things even if they never noticed this, and mainly for accept me as I am and never judge me for this. Also to my classmates in the metrology laboratory: David Asael, Silvino, and Cristian Caloca; for sharing many things through all this time.

To all my friends outside from CIO; especially to Ana Lilia Flores, Emma Gutierrez, Dulce Roa, Ruben Garcia, Alejandra Mina, Paola Casillas, Gerardo G. Verduzco, Luis A. Martinez. To all the people that supported and helped me through the hooligan adventure in Loughborough, especially to Patrick Perkins, Sandrine Ammiot and Phil Taylor. Also I want to thank to all those persons who never believed in me, to all of them thank you very much, I am still kicking and alive.

I would like to express my recognition during my doctoral studies and research through the financial assistance of the CONACYT and the University of Loughborough, all my gratitude to those agencies.

# Content

# Chapter I

# 1. Introduction

For many years human beings have been intrigued by the ability of insects, birds and other flying animals because of their interest in reproduce their complex flight system. For centuries humans have registered many studies on them, from a simple tiny fly, to a huge bird. Men have also been interested in some animals that can't fly and do not have the same structure as insects and birds, such as flying fishes, squirrels, frogs and even some snake species. We have tried to copy, reproduce and understand the phenomena involved during flight, and try to apply it in several human inventions.

Most of the winged insects present two pairs of wings, like grasshoppers, bees, wasps, dragonflies, true bugs, butterflies, moths, and many more. Some insects have large wings, such as Dobsonflies and Antlions, and they are considered as poor fliers, while bees and wasps with smaller wings are considered as good fliers [1]. It is worth to mention that not all the wings are involved during flight, a good example of this are the outer pair of wings of beetles, which are quite hard and not functional during flight. The number or wing size are not a determinant reason to classify the flying ability of the insects. There are some flies that belong to a large group of insects with only one pair of wings, although they have small balancing organs known as halteres where a second pair of wings might develop. These halteres vibrate with the wings and sense any changes of wind direction.

Insects' flight ability allow them to survive since they are able to escape from danger, move long distances to live, find food and places to reproduce. The latter involves the efficient use of energy during flight rather than walking due to their small size.

The flight behaviour changes from one species to another, sometimes drastically, since some of them present a clumsy flight pattern like some beetles, and others in comparison present an acrobatic flight capability as dragonflies. One of the most skilled winged insects are flies, they are capable to move forward, backward, sideways, and even up and down [2]. The flight capability is gained by muscles not attached directly to the wings which move them indirectly by changing the shape of the thorax [2].

Some of the facts described above can only explain a few facts about insects' flight, which is a complex system involving many components, for this reason it is necessary to improve and gain a better understanding and knowledge about the complex behaviour of insects during flight. Butterflies were chosen for this work for several reasons including the large number found in the local environment that avoids any adverse effect in their ecosystem: it is in the state of Guanajuato, central part of Mexico, where all butterflies were collected from their natural habitat.

Non-contact optical techniques are mainly applied to measure object surface deformations, allowing indirect calculation of its mechanical parameters and properties. Most of these techniques have higher spatial resolution than their similar and more traditional mechanical counter-parts [3, 4]. DHI is an optical non-invasive method which renders qualitative and quantitative data from an object's displacement [5-9]. DHI has been applied to inspect biological samples as an alternative to traditional invasive techniques [10].

The research reported in this work stems from the interest of scientist and engineers in different engineering design and research areas, e.g. aerodynamics, and hopefully will contribute to improve the knowledge about the insects' flying efficiency and in the future could be applied to the design and development of new flying devices. Because of this, insect wing flapping detection and measurement can provide useful data that can be used to redesign the aero dynamical properties of current aircrafts.

Some previous studies have helped to gain a better understanding about the structures, the shape and behaviour of winged animals, in particular those trying to reproduce the complex characteristics involved in flying. Most of this knowledge has already been applied in modern aerodynamic models which gave way to more efficient airplanes, rockets, etc., [10-12], and has served to enhance physical parameters such as air pressure distribution and friction reduction [13]. In recent years research on flying insects has been primarily focused in the use of newer techniques like computer modelling, new pressure sensors, computational simulation, and flow visualization [14-21]. Further research has developed nano electronic models with complex computer control systems which simulate an insect's flight [22-24]. Photogrammetry is yet another useful technique applied to extract the kinematics of several marked points on an insect wing during tethered and hovering flight [25].

In this thesis an alternative new approach based on a non-contact optical technique, for the study of insect wing deformation during flight is presented. A DHI system with a high speed camera and a cw high output power laser to record fast and non repeatable events [26-28] is employed. Deformation maps acquired during the insect flapping are presented

showing its displacement amplitude. This optical non-destructive technique is used as a feasible alternative to better understand the phenomena of insect wing deformation in events such as up-stroke and the down-stroke wing movements.

The experimental results are presented in chapter 3, showing the changes suffered by the in-flight insect wing, where the measurement is registered over the whole insect wing surface, and not only in a single point of the wing as all non optical techniques report. Also, a time vs. displacement tracking plot of randomly chosen wing sections is presented to show the differences of behaviour among different wing sections of a butterfly during flight. The latter provides an interpretation of the fact that each wing section moves independently in order to compensate any pressure changes or rough changes in flight movement, and how DHI successfully detects these fast and small changes suffered over the whole wing surface. Chapter 4 presents a discussion of the results and the conclusions of this research work.

# Chapter II

## 2.1 Background to Digital Holographic Interferometry (DHI)

Optical metrology uses several laser measurement techniques capable of measuring static, dynamic and even non repeatable events, with very high sensitivity. In this research work High Speed Digital Holographic Interferometry (HSDHI) is the optical non contact technique employed to measure the insect wing deformations. This chapter describes the basic concepts on interferometry, speckle interferometry, Electronic Speckle Pattern Interferometry (ESPI) and Digital Holographic Interferometry (DHI). It also deals with the Fourier transform method to evaluate the relative phase difference maps. The chapter concludes with some basics concepts on flying insects, mainly focused on butterflies.

### 2.1.1 Speckle

When an object with a non smooth surface is illuminated by a coherent light source of wavelength ($\lambda$), such as a laser beam, a granulated appearance can be observed by the scattered light from the object's surface. This optical effect is known as speckle [3, 4]. The random interference pattern is a product of multiple *reflections* that occurred in the object's surface, where de magnitude $\lambda$ is equal or smaller than the height of the inhomogeneities ($\sigma$) [4]. The scattered light phenomenon mentioned above is shown graphically in the Fig. 2.1

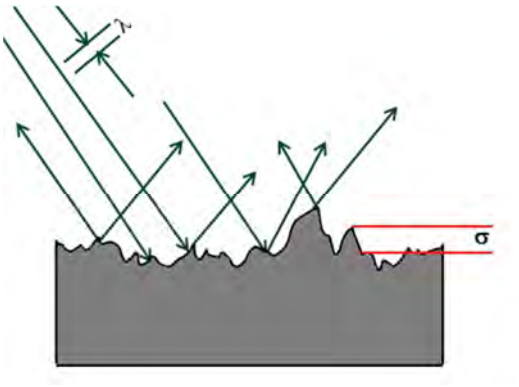


Fig. 2.1 Light scattered by a surface illuminated with coherent light

The scattered light from a surface produces the interference of several wave-fronts that have been individually scattered from neighbouring surface points, forming an interference pattern shown as random bright and dark spots, a cumbersome pattern of light design named speckle that depicts the randomness of the object surface. The speckle effect has an important role in the type of interferometry treated in this chapter since it allows the generation of fringe patterns from the non smooth object (e.g. insect wings) when it is compared between a non deformed, and a deformed state. Fig. 2.2 shows an image of a speckle pattern, where it can be seen that the speckle size varies. To find the speckle size the objective and subjective speckle concepts need to be defined.

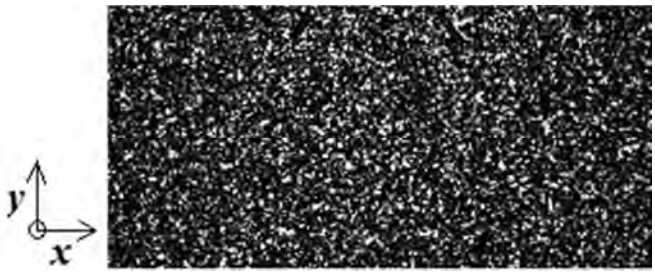


Fig. 2.2 Speckle pattern

### 2.1.1.1 Objective Speckle

The objective speckle is generated when a laser illuminates a surface with an area of section *D* and the speckle is observed on a screen (S) located at a distance (*z*) from the scattering surface, this can be observed in Fig. 2.3.

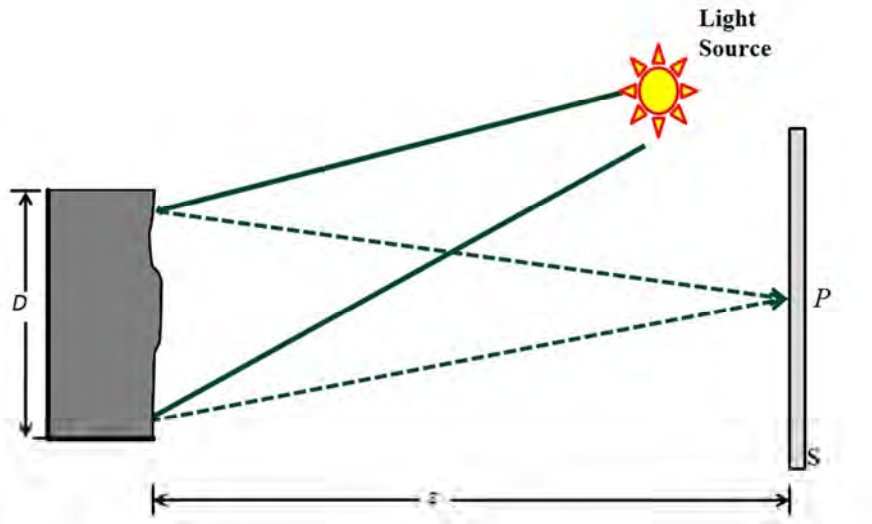


Fig. 2.3 Objective speckle.

Consider an arbitrary point on the observation screen (S) defined by *P*, and assume that this point collects all the contributions from all points on the scattering surface, thus the speckle pattern in *P* is the superposition formed by the scattered light coming from any pair of points from surface. Then any two points in P separated by a distance (*l*), will produce fringes with a frequency given by [3]

$$f = \frac{l}{\lambda z} \qquad \text{Eq. (2.1)}$$

where $\lambda$ is the light source wavelength and $z$ is the distance from the object surface to the observation screen (S), respectively. The maximum spatial frequency ($f_{max}$) is produced from two adjacent points defined by the Eq. (2.2). The pattern period defines the smallest speckle size ($\sigma_o$), which can be approximated using the Eq. (2.3).

$$f_{\max} = \frac{D}{\lambda z} \qquad \text{Eq. (2.2)}$$

$$\sigma_o = \frac{\lambda z}{D} \qquad \text{Eq. (2.3)}$$

### 2.1.1.2 Subjective Speckle

When a surface is illuminated by a coherent light source and an optical element (a lens) is located between the object and the observation screen, an image of the object surface is generated as shown in Fig. 2.4. The two point interference on the screen is now called subjective speckle.

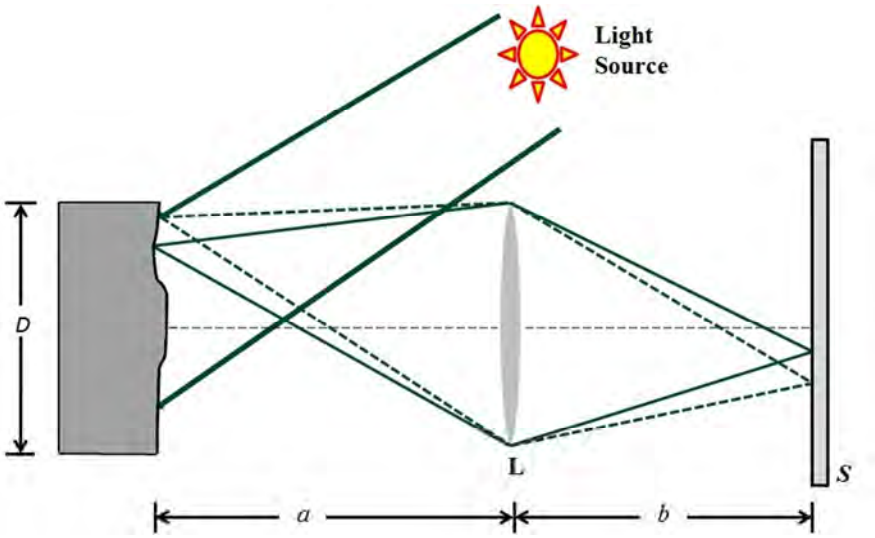


Fig. 2.4 Subjective speckle.

The subjective speckle size can be determined in a similar way to the objective speckle size [3-7], however in this case the transversal section area is limited by the lens diameter ($D_L$) which is the image forming system, then the speckle size is defined as,

$$\sigma_s = \frac{\lambda b}{D_L} \qquad \text{Eq. (2.4)}$$

Where *b* is the distance from the lens to the observation screen. Notice that when the aperture size decreases the speckle size increases, a feature that may readily be observed if one squints when watching directly at the screen.

$$F^{\#} = \frac{f}{D_L} \qquad \text{Eq. (2.5)}$$

The aperture number ($F^{\#}$) is the relation between the lens focal length (*f*) and its diameter ($D_L$); the simpler way to relate the $F^{\#}$ with the magnification (m) of the imaging system, is rearranging Eq. (2.4) as,

$$\sigma_s = (1+m)\lambda F^{\#} \qquad \text{Eq. (2.6)}$$

Where the system's magnification can be expressed as

$$m = \frac{b - f}{f} \qquad \text{Eq. (2.7)}$$

The speckle pattern interferometry method has several important parameters to be taken into consideration, these are: the speckle size, the intensity distribution, the point spread function and the optical system resolution. To obtain better results it is necessary to avoid optical aberrations (particularly spherical or coma) caused by the lenses used in experimental set-ups, since they can introduce errors in the measurements, e.g., a curvature in the borders of the object's surface.

### 2.1.2 Speckle Pattern Interferometry

Speckle Pattern Interferometry (SPI) [3-7] is based on the principle that for displacements, or small surface deformations, the intensity of the components individually dispersed in the resolution area remains constant. This implies that the position of each speckle practically remains equal. Then, the phase of each speckle in the image plane contains the information due to the superficial displacement. If a second wave front is added and is mutually coherent to the speckle fringe pattern, this acts like a phase reference. The intensity of each speckle is then a function of the phase relationship between both wave fronts, which strictly speaking, are related to the superficial deformation. The superficial deformation can be seen like a difference between speckle intensities. Electronic Speckle Pattern Interferometry widely known as ESPI, is a non contact measurement technique that can be used to measure strain, vibration and object's shape, among many others physical, and mechanical parameters [3, 4, 7,8].

As a result of an external agent the changes suffered by the object's surface can be explained as a difference between the speckle intensities, this is when two speckle patterns re recorded, with the first one defined as the non deformed state and the second one as the deformed state. These speckle patterns are compared (correlated) by addition, subtraction or multiplication its intensities, having as a result a bright and dark fringe pattern with an equal phase difference between both, as it is shown in the Fig. 2.5.

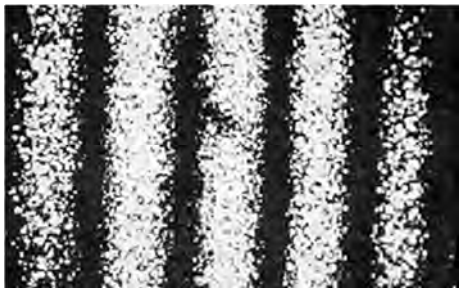

Fig.2.5 Dark and bright fringe pattern

The first recorded interferogram is produced by the interference of the reference and object beams, and they can represented by:

$$U_o = u_o e^{-i\vec{k}_o \cdot \vec{r}}$$

$$U_r = u_r e^{-i\vec{k}_r \cdot \vec{r}} \qquad \text{Eq. (2.8)}$$

Where $u_o$ and $u_r$ are the wave amplitudes, $\vec{k}_o$ and $\vec{k}_r$ are the wave vectors, $\vec{r}$ is the position vector taken from a coordinates reference system. Then the intensity recorded in the interferogram can be expressed by the following equation

$$I = \left|U_o + U_r\right|^2$$

$$I = \left|U_o\right|^2 + \left|U_r\right|^2 + U_o U_r^* + U_o^* U_r \qquad \text{Eq. (2.10)}$$

Where * denotes the complex conjugate term, and equation 2.10 represents the interferogram of the non deformed state or reference state, and can be rewritten as [8]

$$I(x,y) = I_o(x,y) + I_r(x,y) + 2\sqrt{I_o(x,y) I_r(x,y)}\cos\left[\varphi(x,y)\right] \qquad \text{Eq. (2.11)}$$

Where $\varphi(x, y)$ represents the speckle phase that varies with the position $(x, y)$. If a phase change (related with the object deformation) between these two wavefronts occurs, the intensity will also change and this represents the deformed state, and it can be written as

$$I(x,y) = I_o(x,y) + I_r(x,y) + 2\sqrt{I_o(x,y) I_r(x,y)}\cos\left[\varphi(x,y) + \psi(x,y)\right] \qquad \text{Eq. (2.12)}$$

Where $\psi(x, y)$ is the phase introduced by a deformation or displacement suffered by the object surface. Since $\varphi(x, y)$ is a random function of the position, the interference fringes produced by $\psi(x, y)$ cannot be interpreted in a direct form. There are three techniques reported in the literature that render correlation fringes, from Eqs. (2.11) and (2.12) namely

- Correlation by Subtraction
- Correlation by Addition
- Correlation by Multiplication

### 2.1.2.1 Correlation by Subtraction

The correlation by subtraction [4] is obtained performing a subtraction between a non deformed state, known as reference state, represented by Eq. (2.11) and a deformed state which is represented by Eq. (2.12). The difference between these two states is given by:

$$I(x,y) = 2\sqrt{I_o(x,y)I_r(x,y)}\left|\cos(\varphi+\psi)-\cos\varphi\right| \qquad \text{Eq. (2.13)}$$

Correlation by Subtraction can be performed electronically via a frame grabber within a PC, yielding a fringe pattern that can be seen in real time (30 frames /second) on a screen (computer or TV). When Eq. (2.13) is rewritten to eliminate negative intensity values, it produces the next expression:

$$I(x,y) = 4\sqrt{I_o(x,y)I_r(x,y)}\left|\sin(\frac{2\varphi+\psi}{2})\sin\left(\frac{\psi}{2}\right)\right| \qquad \text{Eq. (2.14)}$$

Where sinusoidal terms represent two functions that cross modulate. The first sinusoid term has high spatial frequency (due to speckle noise), and the second has low spatial frequency and is commonly known to give way to correlation fringes. A minimum occurs when the (second sinusoidal) argument takes values given by Eq. (2.15). $\psi$ is related to displacements suffered by the object's surface, and it is a term that allows the calculation of quantitative data.

$$\psi = 2n\pi \qquad \text{Where n= 0, 1, 2,...} \qquad \text{Eq. (2.15)}$$

### 2.1.2.2. Correlation by Addition

The Correlation by Addition [4] can be obtained adding the first recorded non deformed state with the deformed state of the object, and this technique could be useful to observe object movements such as in biological/ human tissue or a mechanical plate, if the images recorded produces a high quality fringe pattern. From Eqs. (2.11) and (2.12),

$$I(x,y) = 2I_o(x,y)I_r(x,y) + 2\sqrt{I_o(x,y)I_r(x,y)}\left|\cos(\varphi+\psi)+\cos\varphi\right| \qquad \text{Eq. (2.16)}$$

Eq. (2.16) can be rewritten to obtain the terms of high and low spatial frequency respectively as

$$I(x,y) = 2I_o(x,y)I_r(x,y) + 4\sqrt{I_o(x,y)I_r(x,y)}\left|\cos(\frac{2\varphi+\psi}{2})+\cos\left(\frac{\psi}{2}\right)\right| \qquad \text{Eq. (2.17)}$$

Where the term of high frequency is the first cosine (due to speckle noise) and the second cosine term is the low frequency, with the minimum fringe intensity occurring when

$$\psi = (2n+1)\pi \qquad \text{Where n= 0, 1, 2...} \qquad \text{Eq. (2.18)}$$

A high DC term, $2I_A(x, y)I_B(x, y)$, appears and makes that the fringe visibility decreases. Fringe patterns can be obtained and recorded electronically using a digital camera sensor, but high frequency noise will be observed: this is why addition is seldomly used.

### 2.1.2.3. Correlation by Multiplication

The Correlation by Multiplication is described by Alcala et al [9], and can be obtained multiplying a first recorded non deformed state with the deformed state of the object, from Eqs. (2.11) and (2.12)

$$I(x,y) = a^2 + \frac{b^2}{2}\cos(2\psi + \varphi) + 2ab\cos(\psi + \frac{\varphi}{2})\cos(\frac{\varphi}{2}) + \frac{b^2}{2}\cos\varphi \qquad \text{Eq. (2.19)}$$

Where a $= I_o(x, y) + I_r(x, y)$ and b $= 2\sqrt{I_o(x,y)I_r(x,y)}$. The last two terms on the right-hand side of Eq. (2.19) correspond to two fringe patterns of different amplitudes, while the other terms represent optical noise. Multiplication is also rarely used mainly due to the intensive computational requirements needed.

## 2.1.3 Sensitivity vector

The speckle random intensity distribution and its optical phase are cobwebs of intricate interference patterns that may be related to object displacements and surface structure roughness [3, 4]. All the terms involved to determinate the sensitivity vector are represented in the schematic drawing in Fig. 2.6.

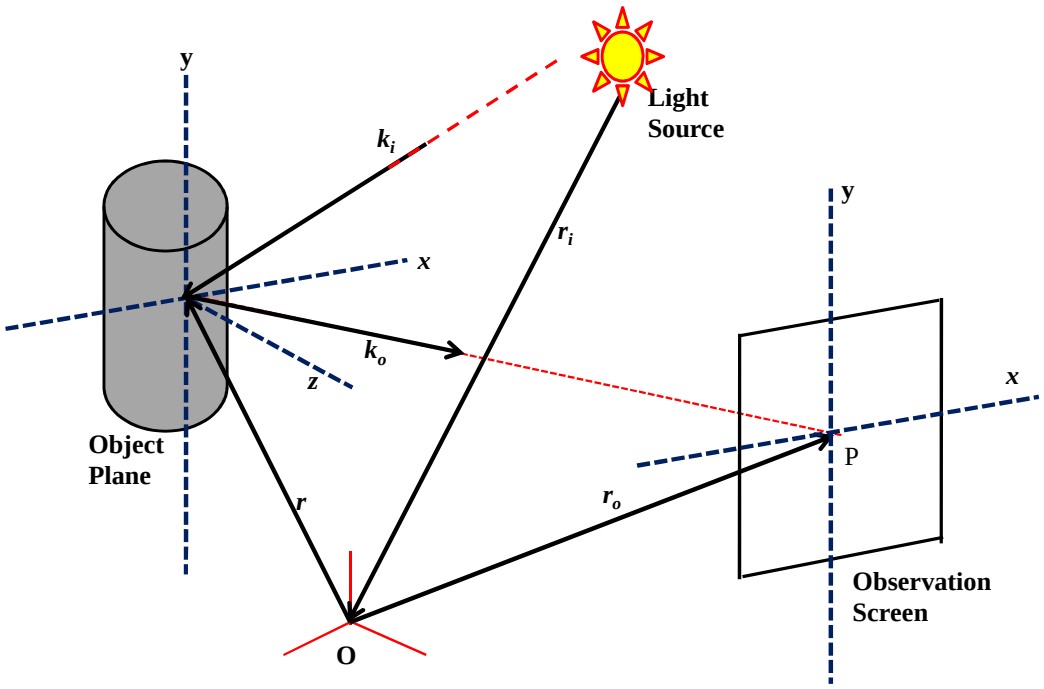


Fig. 2.6 Schematic for the sensitivity vector

From figure 2.6 it can be implied that the optical phase observed at a point P in the viewer's plane (screen), can be expressed as a function of the path followed by the light from the illuminating source to the point P, as follows:

$$\psi = \psi_P + \phi$$

$$\psi = \psi_P + \phi_i + k_i \cdot (r - r_i) + k_o \cdot (r_o - r) \qquad \text{Eq. (2.20)}$$

The complete speckle optical phase is the sum of a random component expressed by $\psi_p$ and another component $\phi$, which is composed by the illuminating source phase $(\phi_i)$ and all the added phase displacements occurred to the light in its way from the source to the

observation point. Phase changes depend on the position vector from the object ($r$) and the position vector from the source ($r_i$), and also from the vector position in the observation plane ($r_o$). Observation and illumination vectors can be defined as

$$\vec{k}_i = \frac{2\pi}{\lambda}\hat{n}_i \qquad \text{Eq. (2.21)}$$

$$\vec{k}_o = \frac{2\pi}{\lambda}\hat{n}_o \qquad \text{Eq. (2.22)}$$

Where $\hat{n}_i$ and $\hat{n}_o$ are the illumination and observation unitary vectors respectively. The sensitivity vector $\vec{k}$ is shown in Fig. 2.7 and is given by

$$\vec{k} = \hat{n}_i - \hat{n}_o \qquad \text{Eq. (2.23)}$$

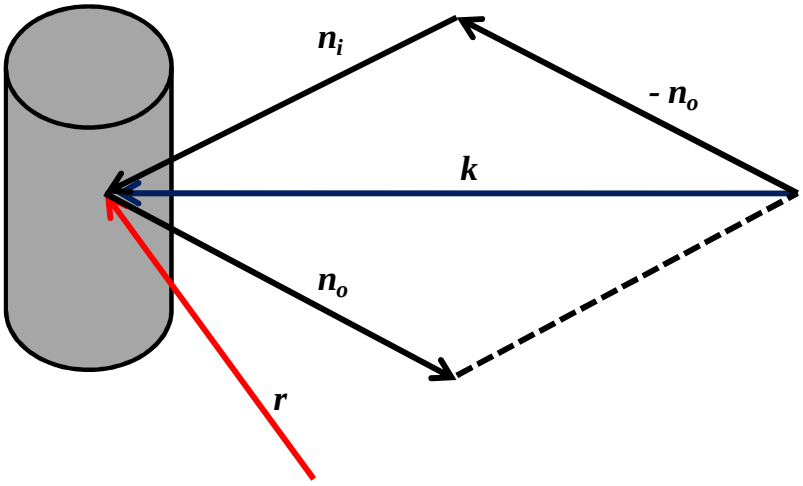


Fig. 2.7 Sensitivity Vector

When the object is modified or the illumination conditions change, the speckle phase also changes, these variations can be expressed by,

$$\Delta\psi = \Delta\psi_p + \Delta\phi' + \Delta\left(\frac{2\pi}{\lambda}\vec{k}\cdot\vec{r}\right) \qquad \text{Eq. (2.24)}$$

Where the term $\Delta\psi_p$ can be considered null, if the changes suffered do not alter in a significant way the micro structure of the object's area. Then the optical phase difference ($\Delta\psi$) can be expressed in an easy way considering the phase sensitivity as a function of the sensitivity vector which is given by;

$$\Delta\psi = \frac{2\pi}{\lambda}\vec{k}\bullet\Delta\vec{r} \qquad \text{Eq. (2. 25)}$$

Where $\Delta\psi$ is the phase difference for one direction of the illumination vector and one for the observation, and it is related with the dot product between the displacement ($\Delta\vec{r}$) and the sensitivity ($\vec{k}$) vectors.

### 2.1.4 Interferometers

Interferometers are optical systems employed to interfere (or overlap) wavefronts coming from a light source, giving as a result fringe patterns which basically are dark and bright intensity contours. They are classified in two main groups: Amplitude dividing interferometers and wavefront dividing interferometers.

The first group divides the primary wavefront in two segments that travel different optical paths before they are recombined, while the second group uses sections from the main wavefront to create a secondary wave front. Amplitude interferometers are commonly used in ESPI, DHI and other interferometric systems to produce interference fringes that are directly related to the displacement or surface changes by an object under test. The best example of an Amplitude interferometer is shown in Fig. 2.8, known as Michelson interferometer [32, 33]. These types of interferometers can be configured to measure in-plane and out-of-plane displacements.

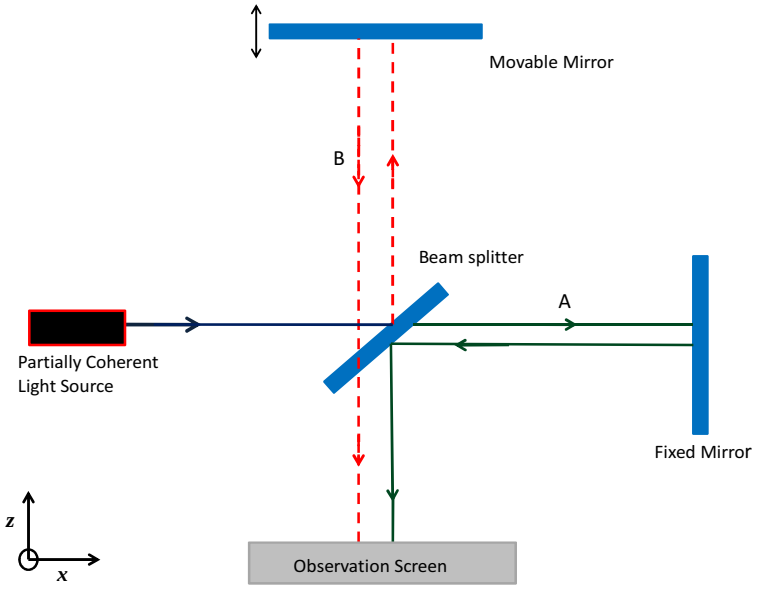


Fig. 2.8 Michelson Interferometer

### 2.1.4.1 Out-of-plane and In-plane Interferometers

The out-of-plane interferometer [3, 4], consist of an optical set up capable to measure displacements mainly along the normal to the object surface (see Fig. 2.9).

The out-of-plane interferometer sensitivity is determinate and controlled by the angle $\theta$ formed between the normal to the observation plane (or camera sensor) and the principal axis of the wavefront coming from the light source. Fringe contrast increases as the optical path difference *(opd)* approximates to zero [4], and the displacement measurement is given by

$$d = \frac{\lambda}{2\pi}\frac{\Delta\psi}{2\left(1+\cos\theta\right)} \qquad \text{Eq. (2.26)}$$

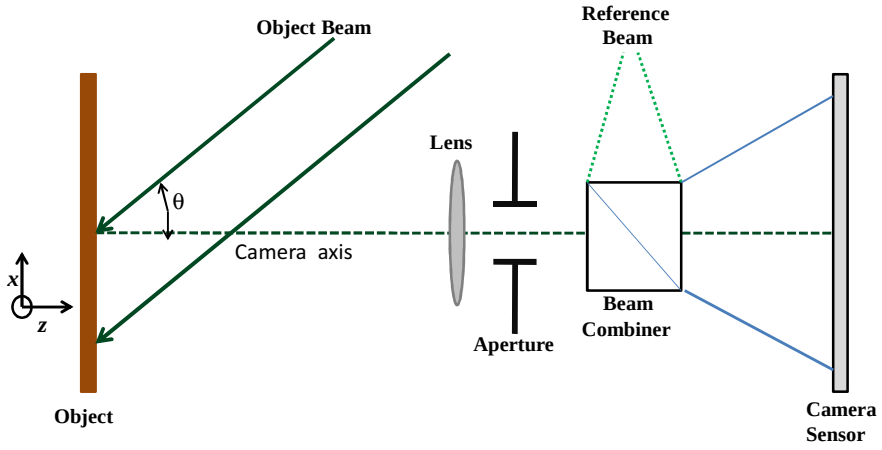


Fig. 2.9 Out-of-plane interferometer

On the other hand, the in-plane set-up described in the literature has a sensitivity to detect changes or displacements along the plane perpendicular to the normal to the observation direction, as can be seen in Fig. 2.10.

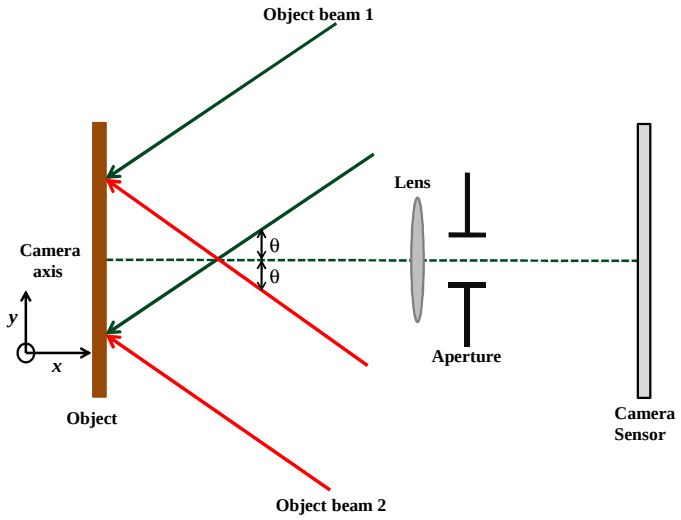


Fig. 2.10 In-plane interferometer

The in-plane interferometer's sensitivity depends on the angles formed by the object illumination beams with respect to the normal to the observation plane, both angles ($\theta$) are equal (but opposite). If the angle value is small, then larger displacements can be detected, but if the angle value is large then it can be used to measure small displacements *(d).* The latter is expressed by the next equation [4]:

$$d = -\frac{\lambda}{2\pi}\frac{\Delta\psi}{2\sin(\theta)} \qquad \text{Eq. (2.27)}$$

## 2.1.5 Digital Holographic Interferometry theoretical concepts

Digital Holographic Interferometry is a non contact and non invasive measurement technique with high sensitivity and high spatial resolution, capable to detect displacements (deformations, vibrations, etc.) over an object under test in a qualitative and quantitative way.

DHI measures displacements using a digital camera sensor like CCD or CMOS, which detects the intensity that is produced by the interference between the object and the reference beams as seen in Eq. (2.10). DHI presents a similar performance to ESPI, i.e. both are based on the same interference principle and use a similar optical set up. However, DHI allows to obtain the wrapped phase with the Fourier transform method using any two digital holograms [35], while ESPI employs techniques like phase stepping [36], needing extra hardware to provoke an optical path difference in the setup, e. g., using a piezoelectric attached to any mirror in the optical setup. DHI shows a higher spatial resolution as compared to more traditional mechanical tests [3, 4]. It is applied to measure static or dynamic changes suffered by an object, and allows detecting changes in the range of micrometers and nanometers.

From De la Torre [34, 40], DHI may well be presented in a flow chart that contains all steps involved to complete the measuring procedure, see Fig. 2.11. In this figure the reference state hologram (a) and the modified or deformed stated (b) are recorded and stored in a computer. Then both holograms are Fourier transformed [35], and a filtering process is performed to obtain the phase difference. After processing the individual interferograms, the result of the comparison between them, a wrapped phase map directly related to the object surface deformation is obtained. It is then necessary to apply an unwrapping algorithm in order to recover the displacement and phase values to finally quantify the real values of the deformation or displacements suffered by the object's surface.

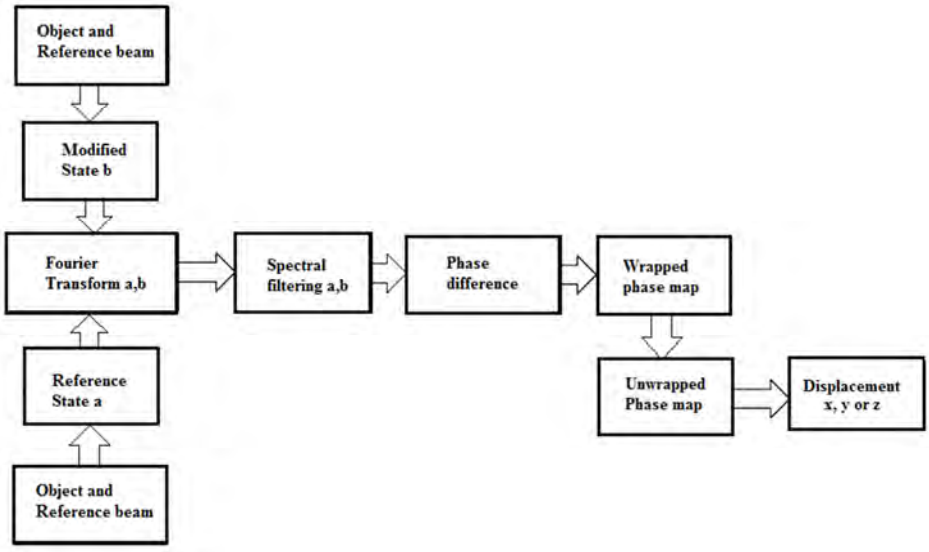


Fig. 2.11 Digital Holographic Interferometry Stages to obtain deformations from an object under testing.

## 2.1.6. Retrieving the Optical Phase using the Fourier Transform Method

Data obtained from digital holographic interferometry needs to be processed by a suitable method to code and decode the different digital holograms recorded. The Fourier transform method is used to evaluate the optical phase and is applied to fringe patterns with sinusoidal behaviour and a carrier spatial frequency. The Fourier transform method used in this work is described by Takeda [35], however is worthy to mention that a previous paper by I. Yamaguchi maybe be regarded as the first paper on the subject [37-39], and both are widely known and used for phase extraction. The phase can be evaluated from interferograms recorded using the next interference relationship which is based in Takeda's Fourier transform method for a single fringe pattern and is given by

$$I(x,y) = \left|I_r(x,y)\right|^2 + \left|I_o(x,y)\right|^2 + I_r(x,y)I_o^*(x,y) + I_r^*(x,y)I_o(x,y) \qquad \text{Eq. (2.26)}$$

Where $I(x, y)$ represents a fringe pattern, the terms for $I_r(x, y)$ and $I_o(x, y)$ refer to the reference and the object beam intensities respectively, while $f_{cx}$ and $f_{cy}$ are the carrier spatial frequencies defined as

$$I_r(x,y) = \left|I_r(x,y)\right| e^{-i2\pi(f_{cx}x + f_{cy}y)}$$
$$I_o(x,y) = \left|I_o(x,y)\right| e^{i\psi(x,y)} \qquad \text{Eq. (2.27)}$$

Eq. (2.26) in its complex form can be rewritten as

$$I(x,y) = a(x,y) + c(x,y)e^{i2\pi(f_{cx}x+f_{cy}y)} + c^*(x,y)e^{-i2\pi(f_{cx}x+f_{cy}y)} \qquad \text{Eq. (2.28)}$$

Where $a(x,y) = \left|I_r(x,y)\right|^2 + \left|I_o(x,y)\right|^2$ and $c(x,y) = I_r(x,y)I_o(x,y)e^{i\psi(x,y)}$ and * denotes the complex conjugate. Applying the Fourier transform to Eq. (2.28) gives:

$$\hat{I}(f_x, f_y) = A(f_x, f_y) + C(f_x - f_{cx}, f_y - f_{cy}) + C^*(f_x + f_{cx}, f_y + f_{cy}) \qquad \text{Eq. (2.29)}$$

Where (^) indicate the Fourier transform, and the carriers ($f_{cx}$, and $f_{cy}$ ) have a magnitude that is large enough to split the average intensity spectrum from the fringe pattern and its convolution with the complex visibility. The Fourier transform of Eq. (2.28) produces three distribution terms shown in Fig. 2.12. To obtain the visibility complex term [35] it is necessary to apply a band pass filter, as shown in Fig. 2.12.

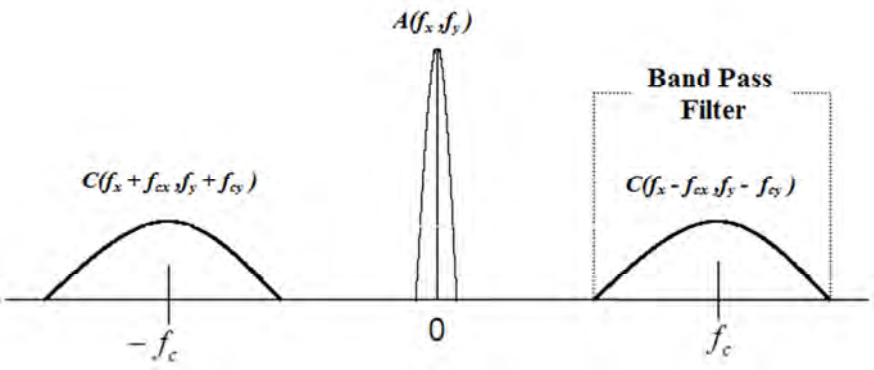


Fig. 2.12 Fourier transform intensity distribution to obtain the phase

After the Fourier transform is calculated, the Eq. (2.29) can be expressed (after filtering and anti-transforming the C($f_x$ - $f_{cx}$ , $f_y$ - $f_{cy}$) term) applying the inverse Fourier transform as:

$$I(x,y) = I_r(x,y)I_o(x,y)e^{i\left[\psi(x,y)+2\pi(f_{cx}x+f_{cy}y)\right]} \qquad \text{Eq. (2.30)}$$

From the above equation the sum of the phase and the carrier can be expressed as

$$\psi(x,y)+2\pi(f_{cx}x+f_{cy}y) = \tan^{-1}\left\{\frac{\mathrm{Im}\left[I(x,y)\right]}{\mathrm{Re}\left[I(x,y)\right]}\right\} \qquad \text{Eq. (2.31)}$$

The carriers can be eliminated from Eq. (2.31) using a known value for $f_{cx}$ and $f_{cy}$ in the time domain, but in the spectral domain, the $\hat{I}(x,y)$ spectrum can be moved to the frequencies axes domain origin ( *I(0,0)* ) before the inverse Fourier transform is performed. Otherwise, if the $\hat{I}(x,y)$ spectrum is inverse Fourier transformed with the $f_{cx}$ and $f_{cy}$ there is not an adverse effect in the relative optical phase difference.

The wrapped phase contains the deformation values codified between -π and π, and it needs to be unwrapped in order to recover the real deformation (amplitude and phase) values of the changes on the object surface , the latter can be expressed as [8]:

$$\Delta\psi(x,y) = \tan^{-1}\left\{\frac{\mathrm{Im}\left[I(x,y)\right]}{\mathrm{Re}\left[I(x,y)\right]}\right\} \qquad \text{Eq. (2.32)}$$

The relative wrapped phase for a series of consecutives images may be found if Eq. (2.32) is rewritten as:

$$\Delta\psi_n(x,y) = \arctan\left\{\frac{\mathrm{Re}\left[I_{n-1}(x,y)\right]\mathrm{Im}\left[I_n(x,y)\right] - \mathrm{Im}\left[I_{n-1}(x,y)\right]\mathrm{Re}\left[I_n(x,y)\right]}{\mathrm{Im}\left[I_{n-1}(x,y)\right]\mathrm{Re}\left[I_n(x,y)\right] + \mathrm{Re}\left[I_{n-1}(x,y)\right]\mathrm{Im}\left[I_n(x,y)\right]}\right\} \qquad \text{Eq. (2.33)}$$

Where $\Delta\psi_n$ is the relative wrapped phase between a reference state hologram ($I_{n-1}(x, y)$) and any other n-th deformed state hologram ($I_n(x, y)$).

## 2.2 Butterfly Background and Basic Morphology Concepts

Humans have been interested in studying birds and insects in flight since many years ago, many have been the main objectives, but in particular some researchers are looking to apply the gained knowledge of these complex systems to improve the design of aerodynamic flying models in order to reduce the air pressure change and friction under, for instance, airplane wings [11, 12].

Interest also lies in studying insect wing motion using for example computer modelling and pressure change measurements with accelerometers and flow visualization. The use and development of nano-electronic models and computer control systems, allow researchers to simulate the behaviour of insect wings at different times. Other measurement techniques use air flow currents to determinate the air changes provoked by the insect wings movements [13]. Also the constructions of fluid dynamic models and visualization have permitted the study of Leading Edge Vortex in wings. Besides this modelling, engineers today are able to construct micro-robotic models using this concept [15-22].

Insects typically move about by walking, flying and occasionally swimming, but the interest is on the winged ones, and their ability to fly. Among all the families of insects there are four main species: Coleoptera, Diptera, Hymenoptera and Lepidoptera [23].

Coleoptera includes all the common beetles but only a few of them can fly, and they mainly use the hard wings as a cover for the back part of the body. The Diptera family, also named true flies, includes flies, mosquitoes gnats and midges: all of them possess a pair of wings. The Hymenoptera includes sawflies, wasps, bees and ants, their wings are transparent and they are considered “heavy” making reference to their family name [23]. Butterflies and moths belong to the Lepidoptera family and since they are present in the local environment in different sizes, shapes and colors, we considered them as the preferred subject to perform the deformation study proposed in this thesis. Butterflies are the subject to be tested, it is then extremely important to describe the main characteristics of the butterflies’ anatomy and some of the phenomena related to its complex flying system.

### 2.2.1 Butterfly Body Parts

Before insects reach the status of winged insects in their adult age, they follow a life cycle, called holometabolism or complete metamorphism. This term is applied to the insect groups that describe four life stages, the first as an embryo or egg, going to larva, and then to a pupa and finally to imago or adult stage (see Fig 2.13). The embryo is from the fertilization of the egg inside the mother until the embryo hatches [24].

The second stage is from birth until the larva pupates. In this part of the cycle this worm-like form can be one of several varieties, most common are: eruciform (caterpillar), scarabaeiform (grub), campodeiform (elongated, flattened, and active), elateriform (wireworm) or vermiform (maggot). Also in this part of the insect's metamorphosis it grows, gains and stores enough energy for the metamorphosis. Then the pupal stage goes from pupation until eclosion, a couple of remark facts are the reduction of movements and that they are often sealed within a cocoon [24].

There are three types of pupae: obtect, exarate or coarctate, where in the obtect the insect appendage is adhered to the body by means of a secretion produced at the last larval moult, while in the exarate the wings and legs are free from the body and the abdomen is movable, and finally in the coarctate, the exarate pupa occurs within the hardened, and tanned cuticle [24]. Inside the pupa the insect suffers internal drastic changes. Finally in the fourth stage the insect emerges from the chrysalis usually having wings and enters to reproductive stage for adult butterfly or imago [24].

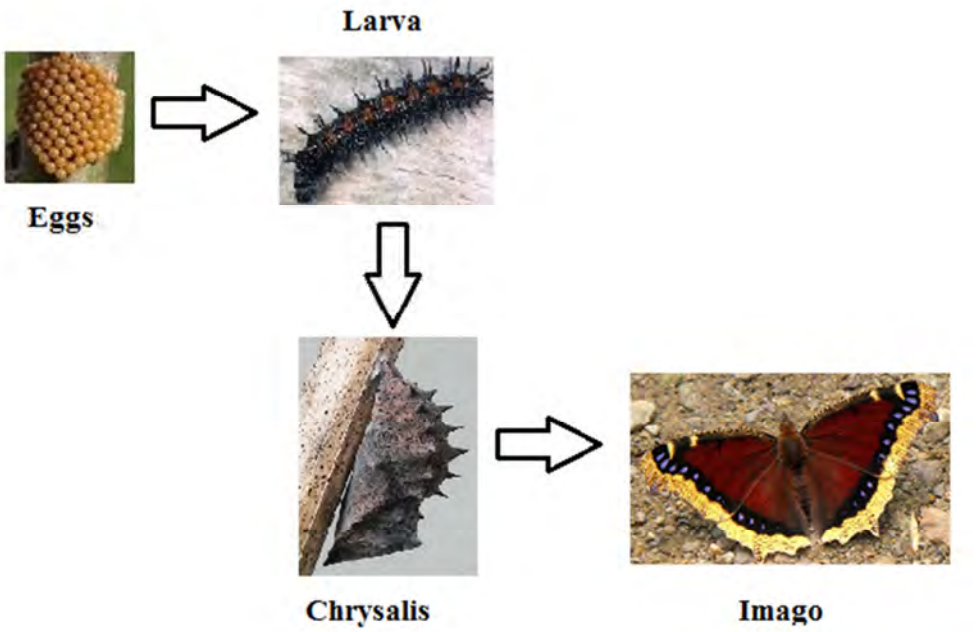


Fig. 2.13 Holometabolism stages or butterfly life cycle.

Once the Imago presents the wings, its body can be divided into three segments or parts (see figure 2.14), namely the head, the thorax and the abdomen [41]. The head contains the eyes, the proboscis, and the antenna. The butterfly's proboscis can be called a tongue, which is uncoiled or unrolled, and it is used to drink nectar from plants or other nutrients. Butterflies use their antenna as a nose, mainly to sniff the air around it. The antenna has a club shape, while in contrast a moth's antenna is feathery. The thorax is the middle section of a butterfly's body which has attached to it the wings and legs. A butterfly has six legs and uses them to probe the surface of a petal and to scratch it. The smallest butterfly's wingspan is about 1/8 of an inch long while the largest one is over 11 inches.

The abdomen contains the butterfly's reproductive organs [41]. The organs that digest food and that get rid of waste products are also located here. The spiracles are the respiratory openings on the thorax and abdomen that allow air to enter the trachea.

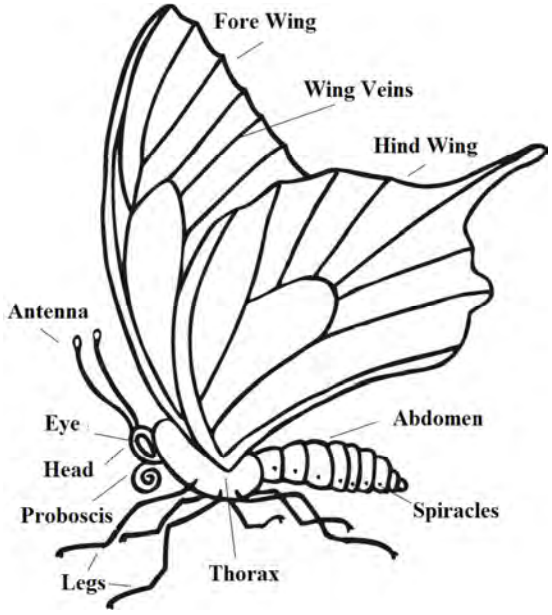


Fig. 2.14 Butterfly body parts.

## 2.2.2. The Wing Structure

One of the main factors for the winged insects to survive on earth is their flying capability [42], they are considered a nearly perfect mechanical machine with different functions and mechanisms [43]. The insect at an adult age presents wings with a flat appearance and well structured vein system. Butterflies and moths have a pair of forewings and hindwings that move as one. They have a kind of sensors that control their wing movement [44]. Insect wings structure is semi transparent, and sometimes it can be coloured by epidermis pigments.

The Lepidoptera family presents scales with a texture similar to the human hair, giving to the wing a soft appearance to the touch. Scales on wings are overlapped one over the other creating groves which act as a whole unit. Scales have a concavity where the pigments that provide colour are found. The wing colour sometimes depends on the scales direction. The scales not only provide a colourful texture to the wing, they are also involved in the flight movements since they play an important role helping to smooth the air flux over the body and wing surface [44].

Wings are water resistant due to a spindle like microform on the scales [44, 45]. It is also worth mentioning that wings have a very important function as a body temperature regulator according to their position. The wings also are capable to displace an air amount that generates the required lift to support the insects' body and allow it to move in several positions and directions. Furthermore, only 0.5 to 5 % of the insects' body weight is used to beat the force generated by the air surrounding its wings. It also helps to compensate the acceleration and deceleration caused by its own mass, this action is repeated several times per second [46].

The wings have a passive response due to the fact that their structure has not a complete muscular control: it is supported by a vein system that creates the wing structure, and they suffer large amplitude deformations particularly when the flapping is slow [47]. The structure varies from male to female, with that of the female body having a more resistant central structure naturally prepared for egg carrying [47].

Fig. 2.15 shows the wings main areas of butterfly forewing and hindwing, both are divided in Basal, Discal, Postdiscal and Submarginal areas covering several cells of the wings, where “cell” in this case is an area bounded by wing veins. The spatial pattern of veins on insect wings is relatively constant for all species and general within a taxonomic family, although it differs greatly among families [48] (more detailed information may be found in Appendix A where a glossary of terms is introduced).

The Lepidoptera Order has nearly 11,000 species including butterflies and moths. The butterflies have daylight habits and moths are nocturnal and attracted to light. Many butterflies species have migratory habits and travel long distances, in some cases distances of over 3000 km, sometimes reaching 3000 m height during their migration flight [41].

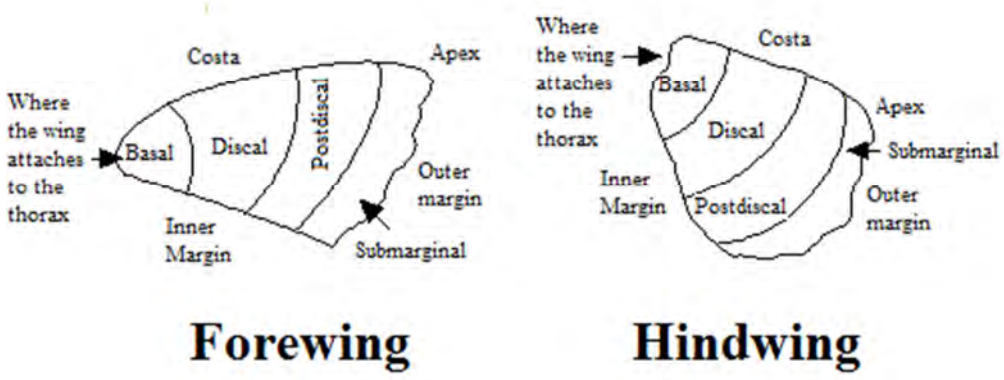


Fig. 2.15 Butterfly main wing sections.

## 2.2.3 Selected Butterflies

The Coleoptera, Hymenoptera and Diptera families present semi-transparent wings and only Lepidoptera presents a colourful wing surface that is useful to obtain backscattering light from them, and this is one of the main reasons to choose butterflies over the other insects as the subject to perform measurements over the wings. Beside the reason mentioned above, the availability and easier to trap and manipulation of them are factors to consider butterflies as the best option to be studied.

In this section the main characteristics of the butterfly species selected for this research are presented. It is worth to remark that there is a vast number of winged insect species (particularly butterflies and moths) in Mexico to provide enough subjects to perform an insect wing study without affecting or endangering any of the chosen species [41, 47- 51]. Figures 2.16(a) to 2.16(e) show the images of the selected butterflies:
(a) *Pterourus multicaudata (Lepidoptera: Papilionidae*) or Eastern Tiger Swallowtail, (b) *Nymphalis antiopa (Lepidoptera: Nymphalidae)* commonly known as Mourning Cloak, (c) *Agraulis vanillae Incarnata (Lepidoptera: Heliconiidae)* known as Gulf Fritillary, (d) *Danaus gilippus Cramer (Lepidoptera: Danaidae)* also called Queen Butterfly, and (e) *Precis evarete Felder (Lepidoptera: Nymphalidae)* known as Buckeye Butterfly. Please refer to Appendix B to check the Taxonomy of each butterfly mentioned above.

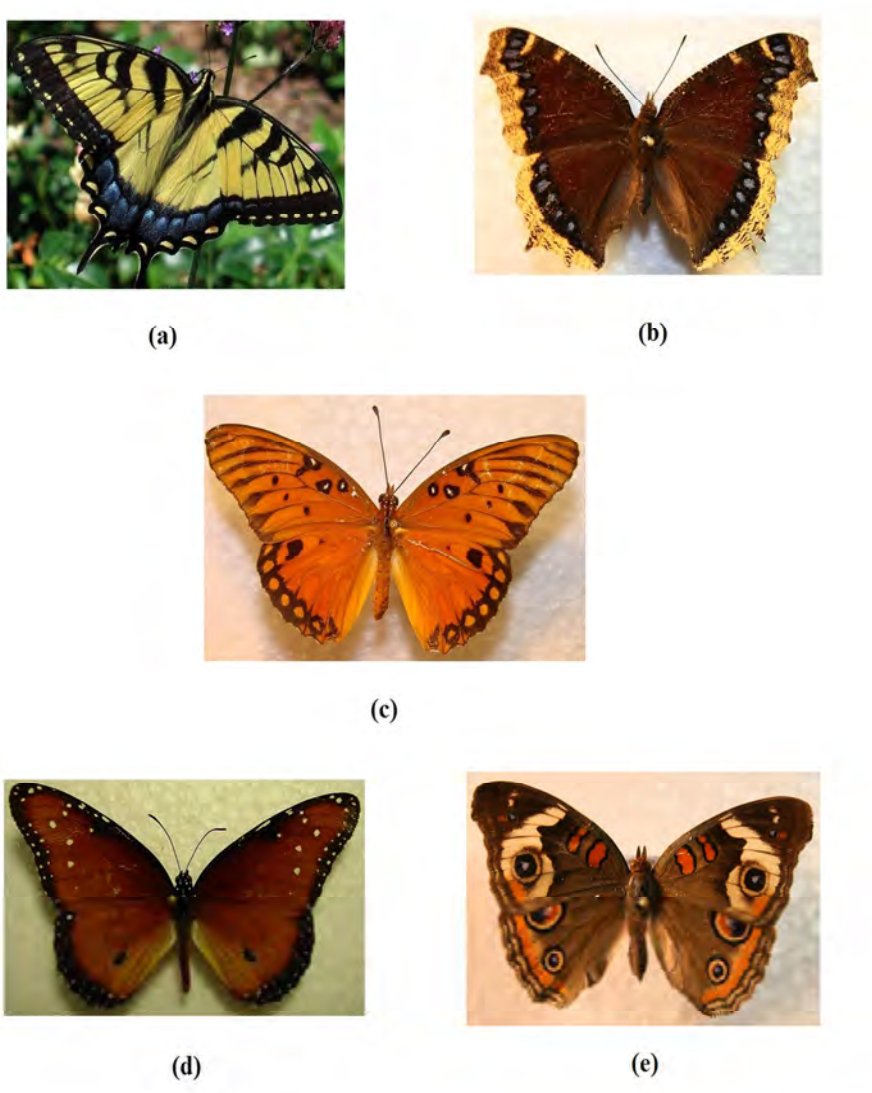


Fig. 2.16 (a), (b), (c), (d) and (e) Butterflies selected from the local environment.

All these butterflies can be found in tropical rainforests and perennial forests through several Mexican regions. These butterflies specifically were collected near the location of the Centro de Investigaciones en Optica A. C. (CIO), and around the city of Irapuato (60 km south of CIO). They were captured with the help of an entomologist, who knows how to trap and keep them alive to perform the experimental tests in the laboratory.

### 2.2.3.1 Butterflies Habits

All winged insects have different characteristics, size, colour, wing form, scales, migratory habits, and of course different flight behaviour. In what follows a brief description about the main characteristics of the Lepidoptera Order chosen for this work is given (Fig. 2.16).

#### 2.2.3.1.1 The Eastern Tiger Swallowtail Butterfly

The Eastern Tiger Swallowtail (Fig. 2.16a) botanically named *Pterourus multicaudata* (Lepidoptera*: Papilionidae*) can be found in various habitats, such as woodlands, woodland openings, woodland edges, fields, open areas, rivers, creeks, roadsides, gardens, urban parks, and city yards. There are two morphs of adult females, a yellow one and a dark one, the yellow one is similar to the male with the exception that there is a patch of blue on the hind wing for the male. The Eastern Tiger Swallowtail is seen from February to November, and it uses a wide range of food sources. Most adults prefer the nectar on sturdy plants, while males are attracted to mud, damp gravel, and puddles, extracting sodium from these sources, also have been seen feeding on dung, carrion, and urine [52].

#### 2.2.3.1.2 The Mourning Cloak Butterfly

*Nymphalys Antiopa (*Lepiddotera*: Nymphalidae),* known as The Mourning Cloak (see Fig. 2.16b) is found in all Mexico, but mainly in cold and template zones, and its migratory term is from February to June.

The Mourning Cloak has short projections on both wings, irregular border, and the upper side is purple-black with a wide, bright yellow border on outer margins, and a row of iridescent blue spots at the inner edge of the border. The adult specimens have a fast flight, feeding themselves from tree sap and rotting fruits, while the caterpillars of this butterfly get their food from willow tree leaves. These butterflies have their adult life period on winter [49].

### 2.2.3.1.3 The Gulf Fritillary Butterfly

Fig. 2.16c shows an image of *Agraulis vanillae Incarnata (*Lepidoptera*: Helliconiidae)* commonly known as the Gulf Fritillary. This butterfly is patterned on the wing under side and has shiny silver spots across the wings and a rich rose patch at the base of the forewing. It can be found in the central part of México and South America. The caterpillar feeds on plants such as maypop, blue passionflower and corky-stemmed passionflower. The adult tends to feed on tall verbena, pentas, tread softly, drummond phlox, and lantana. This butterfly continuously breeds and it can be seen nearly every month, although the butterfly is most commonly found in September. [49].

### 2.2.3.1.4 The Queen Butterfly

*Danaus gilippus Cramer (*Lepidoptera: *Danaidae)* also called Queen Buttefly (Fig. 2.16d), has a smooth and slow flight, and it can be found over desertic or semi desertic zones from the Mexican estates of Chihuahua, Nuevo Leon, Guanajuato and Queretaro. It can have orange or brown with black wing borders and small white forewing spots on its dorsal wing surface, and reddish ventral wing surface fairly similar to the dorsal surface.

The ventral hindwings have black veins and small white spots in a black border. The male has a black androconial scent patch on its dorsal hindwings. Poplar tree leaves, milkweeds and milkweed vines provide feeding for the caterpillar, while adults are fed with nectar from flowers including milkweeds, fogfruit, and shepherd's needle. The migratory period of this butterfly goes from July to October [49].

### 2.2.3.1.5 The Buckeye Butterfly

The last one shown in Fig. 2.16e is the *Precis everete Felder (*Lepidoptera*: Nymphalidae)* or Buckeye Butterfly, it has an upper side brown, and the forewing with two orange cell bars and two eyespots. Part of a white subapical band appears in the largest lower eyespot, while the hindwing has two eyespots: the upper one is the largest and contains a magenta crescent. In the underside the hindwing is brown or tan in the wet season (summer) and rose-red in the dry season (fall). It feeds from nectar, aster, chicory, gum weed, knapweed, and tickseed sunflower, dogbane and peppermint. The migration term is from May to October and its habitat is in the woodlands, the woodland openings, the woodland edges, fields, and open areas in the Mexican States of San Luis Potosi, Guanajuato, Puebla, Veracruz, Oaxaca, Morelos, Guerrero, Colima and Chiapas. Its migratory period goes from June to November [49].

# Chapter III

# 3. Experimental procedure

The experimental procedure and the results obtained from the different tests performed on the butterflies' wing surface measurements are presented in this chapter.

## 3.1. Experimental set up for DHI

The experimental method followed to do the measurement on the insects' wings deformation (or displacement) was the non contact or non invasive optical technique commonly known as Digital Holographic Interferometry [53, 54, 56-58]. The Digital Holographic Interferometry set up is shown in Fig.3.1. For the experiments camed out throughout this thesis work it uses a continuous wave (cw) VERDI laser source with a wavelength of 532 nm, with a coherence length well over 10 mts and a maximum output power of 6 watts. The light is divided in two beams by the 50:50 beam splitter (BS), one of them is used to illuminate the insect wing and the other is directed towards the CCD sensor and is called the reference beam. The backscattering coming from the object is then collected by means of a 125 mm focal length lens (L) located behind an aperture (A). The reference beam is launched into a single mode optical fibre and is combined with the object beam using a beam combiner (BC) in front of the camera sensor (CCD).

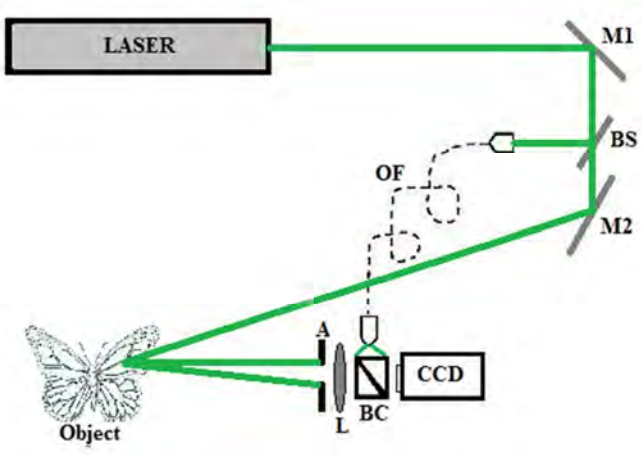


Fig.3.1 Schematic Digital Holographic Interferometry set up. From the figure, (M1) and (M2) are mirrors, (BS) is a Beam splitter, (OF) an Optical fibre, (A) an Aperture, (L) a Lens and (BC) a Beam combiner.

The CCD is a PCO Pixelfly camera with 1392 x 1024 pixels at 12 bits dynamic range, able to capture images at 11.5 frames per seconds (fps). The first image captured is called the reference or base state, and the consecutive images are considered to be the displaced/deformed states. As a proof of principle, the first insect under test is a mosquito known as Crane Daddy Crazy Longlegs (*Tipulidae Oleacera*), and the second insect is the butterfly known as Eastern Tiger Swallowtail (*Pterourous Multicaudata*), see Fig. 3.2(a) and (b).

As it was mentioned in the previous chapter each pair of recorded digital holograms generates a correlation fringe pattern on subtraction, however each digital hologram is individually Fourier transformed to obtain on subtraction with the other hologram the phase information from the wing displacement along the z axis as it is shown in figures 3.3 and 3.4 (a) to (c).

The latter is because the optical setup has an out of plane sensitivity. The mosquito's wing was removed from its main body and placed on a glass slab where it was free to move under random air currents.

In contrast the butterfly was alive during the test and fixed to a wooden slab with a surgical needle, and was able to perform some movements even under the constraint. Both insects were placed on a vibration isolated optical table. Changes on the mosquito and butterfly wings were recorded at different times, with a wing observation area of 18x16 $mm^2$ see Figs. 3.2(a) and (b), respectively.

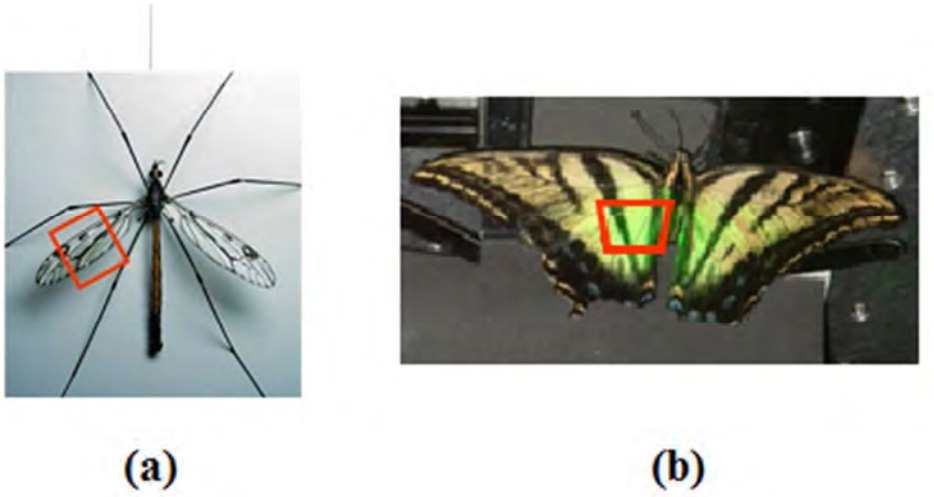


Fig. 3.2 (a) Butterfly and (b) mosquito observation areas for the first set of tests, proof of principle.

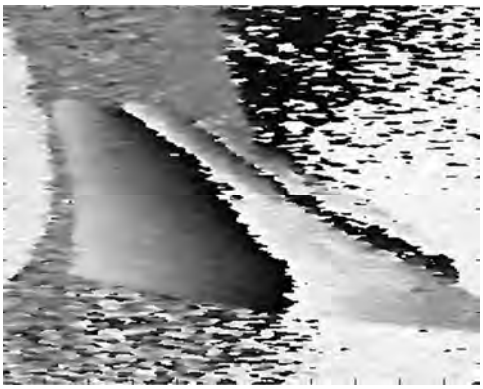

Fig 3.3 Wrapped phase map observed on the mosquito's wing

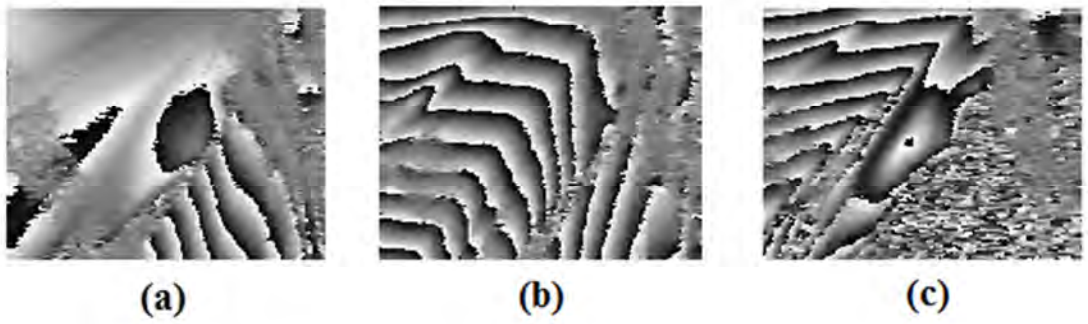


Fig.3. 4 (a), (b) and (c) Wrapped phase maps from different instants of the butterfly's wing.

The noise observed in the wrapped phase maps is produced by several factors: random air currents over the insect wing during the recording; also the wing has an alike human blood circulatory system that produces a surface vibration which changes the speckle behaviour, and besides images were recorded with a low speed camera. After the wrapped phase maps for both insects were obtained, it was necessary to obtain the displacement changes from both the mosquito and the butterfly wings. These results are shown in figures 3.5 and 3.6 respectively, where the displacement is along the *z* axis and the values are normalized to arbitrary units (a. u.).

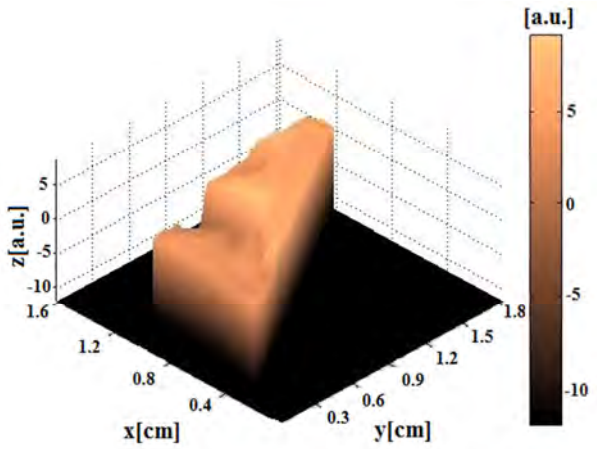


Fig. 3.5 Mosquito wing unwrapped phase map

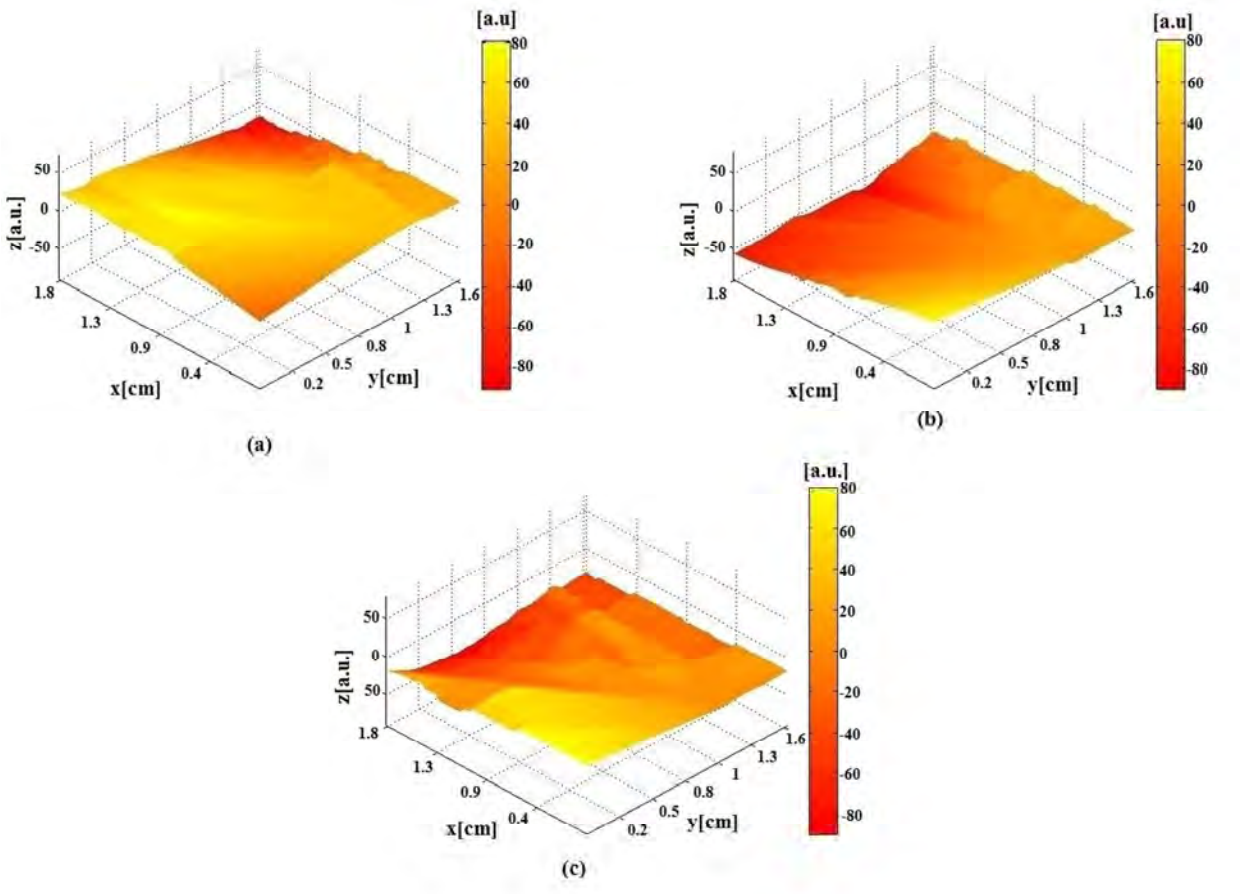


Fig. 3.6 (a)-(c) Butterfly wing unwrapped phase map at different instants.

The unwrapped maps from Figs. 3.5 and 3.6 show the *z* displacement information recorded in the digital holographic interferograms, and represent the displacement changes in the mosquito and butterfly wings respectively. These phase maps show the wing behaviour during particular time instants under the given experimental conditions. After a reviewing the experimental results on the butterfly and mosquito wing described above, and thus proving the fact that DHI can resolve the small changes on the wings due to its high sensitivity and accuracy, the next step is to modify the DHI optical setup to perform several tests over the whole insect's wing surface during the flapping movement in order to gain a better understanding of the flying phenomenon and its complex system.

## 3.2. Experimental set up for High Speed DHI

The previous section serves as a proof of principle to show that measurements on these type of biological samples is possible. To record the natural wing movement and perform in-vivo experimental measurements on the butterfly, in this stage the insect is not pinned, thus avoiding killing it, and is carefully fixed onto a rigid surface taking care to avoid any wing damage, and hence being able to perform the tests under the best experimental conditions with the butterflies alive and ready to be set free at the end of the tests..

In order to obtain the displacement measurements on the whole wing surface, it is necessary to introduce a high speed camera sensor to have a High Speed Digital Holographic Interferometer. High speed DHI makes use of a high speed camera and fast computer processors [55]. High Speed DHI helps to investigate fast and non repeatable

phenomena such as the insect wing displacements during the up-stroke and the down-stroke wing motion.

In this part of the research work an entomologist contributed with his knowledge, teaching us on the way how to capture butterflies and how to keep them alive, also providing us with laboratory containers. He also, lectured us about their anatomy, behaviour and botanical terminology. We thank and acknowledge his invaluable participation in this research work.

The optical set up shown in Fig. 3.1 remains similar, but the CCD camera was replaced with a CMOS camera that allows having high speed recording. The new DHI system is schematically shown in the Fig. 3.7 where the object (butterfly) is illuminated with the same Verdi laser (Coherent V6), using approx. 1.4 W to illuminate the wing, representing an illumination density of 14.6 mW /cm$^2$ on the butterfly.

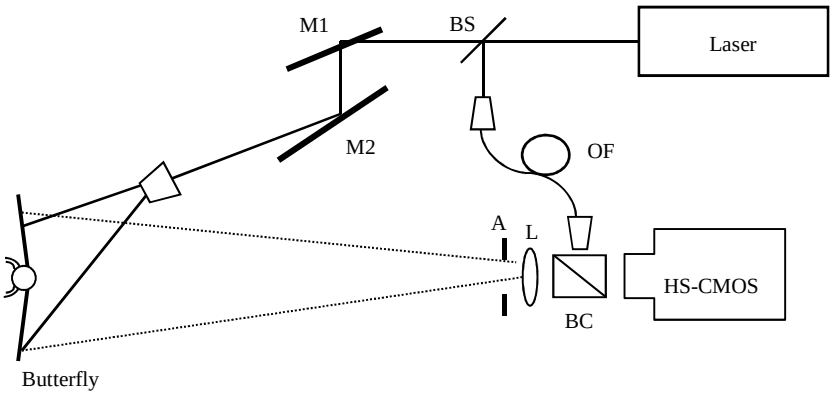


Fig.3.7. Schematic view of the experimental DHI set up with a high speed camera (HS-CMOS).

In order to observe the entire insect the field of view (FOV) is set to image an area of 90 X 100 mm. The interference between object and reference beam is captured using a HS-CMOS high speed camera (NAC GX-1) with an image resolution of 1024 x 1280 pixels at 10 bits dynamic range, this CMOS camera is capable of acquiring 500 frames per seconds using the given characteristics. The butterfly used in this part of the research work was a Pterourus multicaudata (see Fig. 2.16a), which was collected in its pupal stage. After a couple of hours that it emerged from the pupa, a series of tests were performed, at this point the butterfly had a size of 88 X 130 mm of length and width, respectively.

The in-vivo experimental measurement was performed fixing the butterfly onto a rigid surface, trying to avoid any possible damage to the butterfly, or indeed minimizing it. So, each leg was glued to a (dark) metal post and a thread was wrapped around the insect in two contact points such that it was left free to move its wings. The latter procedure avoided the need to use a pin through the butterfly which will certainly modify its wing movements and eventually kill it. This method assured that the butterfly was minimally affected and its wing flapping may be safely considered motion free. Once the insect was located in front of the imaging system, a series of images were recorded at 500 frames per second (fps), which was the ideal CMOS camera frame rate found to perform the experiments, i.e., the required camera repetition frame to momentarily freeze the wing movement.

During the recording process the electronic shutter of the CMOS camera was open, but due to its working characteristics the exposure time is much less than 1 msec. However, the flapping frequency is about 15 times slower than the sampling rate of the camera so the freely flapping (the up and down stroke) movement can be frozen for an instant and the

measurement can be performed. Each experimental test lasted only a few seconds, after which the insect was released and set free. The recorded digital holograms obtained were processed using the Fourier algorithm to each digital holographic interferogram by performing a subtraction between two consecutive holograms, and applying the equation (2.32) the relative phase difference can be obtained. The wrapped phase maps obtained from the latter are shown in Fig. 3.8, and they represent variations through $-\pi$ to $\pi$ (black and white respectively), and represent the insect's wing displacements (at different flapping instants): note that they do not represent the whole amplitude of the flapping movement that is of several centimetres of displacement.

To recover and quantify the real displacement suffered by the insect's wings from the wrapped phase maps show in Fig. 3.8, an unwrapping algorithm was applied to them converting the wrapped phase values to radians. Several unwrapping algorithms are reported in the literature [59-62] and there are other commercially available, but for the characteristic and nature of the images a robust algorithm is needed since a biological sample produces noisy wrapped phase maps. The selected unwrapping method is a minimum cost matching algorithm commercially available: Pv_psua2 software developed by Phase Vision Ltd©. The images refer to micro deformations along the wings between any two consecutive images at 500 fps, i. e., every 2msec. With the information obtained from the wrapped phase maps on the figures 3.8, a continuous out-of-plane deformation map is constructed when the unwrapping is performed on all of them. The corresponding unwrapped phase maps from figures 3.8 are shown in figure 3.9, where the deformation present in the wing's surface goes from -0.9 µm to + 0.9 µm.

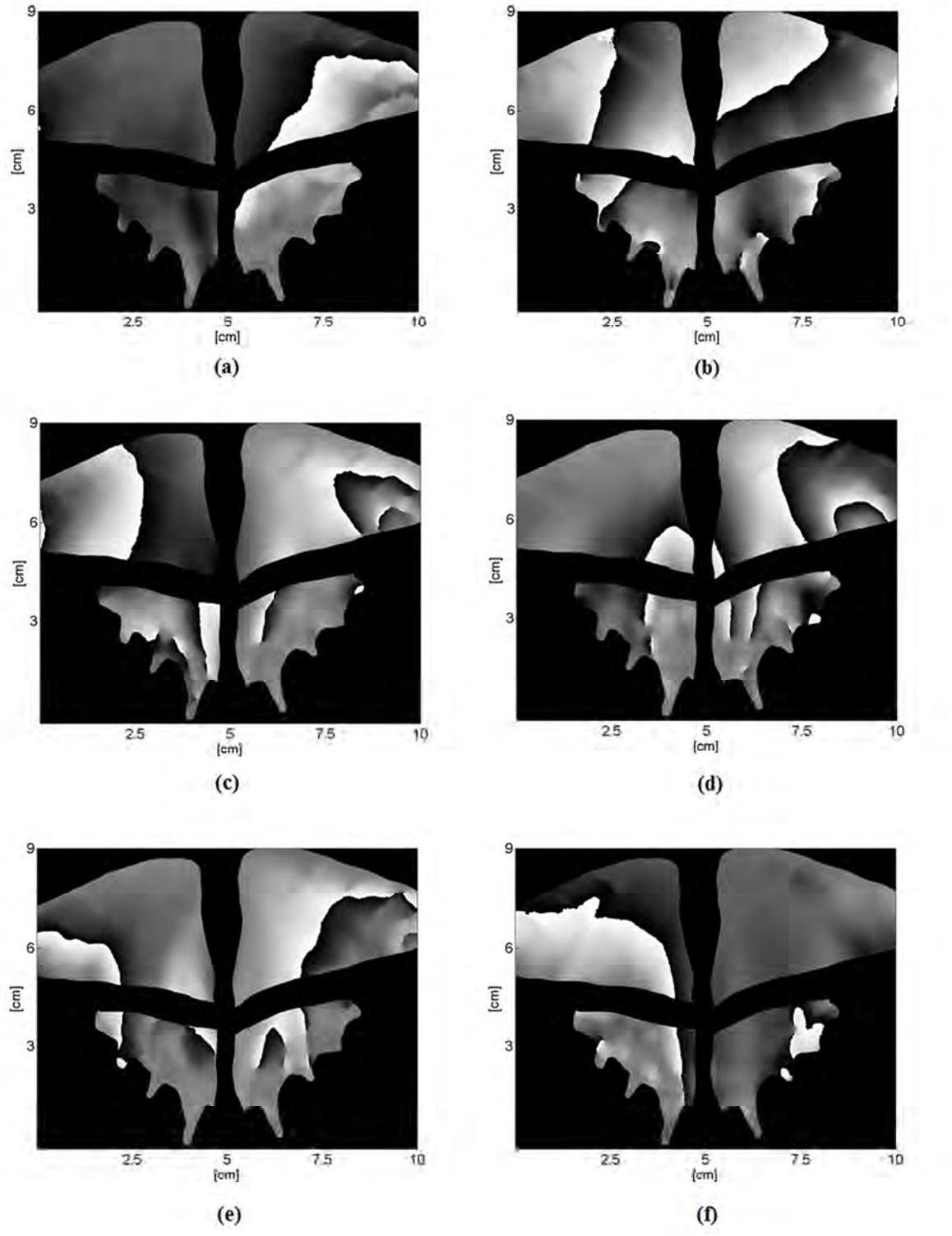


Fig. 3.8 (a), (b), (c), (d), (e) and (f) show the butterfly wing's wrapped phase maps. Each image is for a different time instant during the test which lasts 1.2 secs.

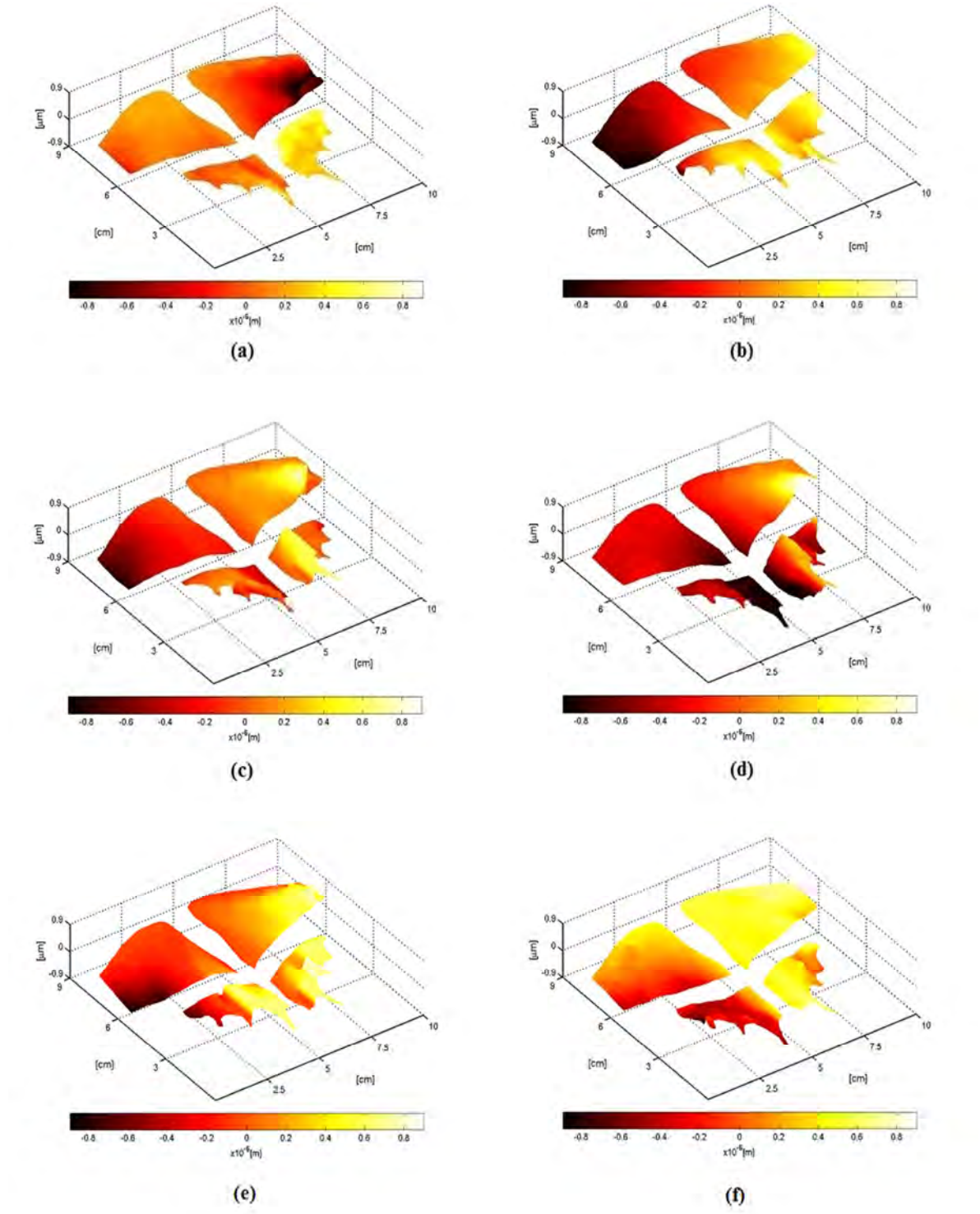


Fig.3.9. (a), (b), (c), (d), (e) and (f) represents butterfly wing surface deformation recovered from DHI measuring experiments at different time instants.

The results presented in this section using an optical technique to observe the full field deformation on butterfly wings during flapping (Figs. 3.8 and 3.9) are to the best of our knowledge for the first time reported in the international literature. From Fig. 3.8 it is possible to observe that the forewing and the hindwing have independent flapping movements, not necessarily symmetric between them.

## 3.3 Comparison on winged insects with High Speed DHI

Section 3.1 demonstrated the usefulness and potential of DHI to study insect's wings flapping in a small area of the wing surface of a butterfly and a mosquito [63], while section 3.2 showed the results for fast and non-repeatable events over the whole wing surface area with data displacements on a micrometric scale [64]. The latter is a step forward to understand the wing motion research, but it was performed only for one specimen and this is not even close to cover the whole information about the Lepidoptera family or the whole winged insect family.

The next step in this research work consisted in performing tests on the specimens Mourning Cloak (Fig. 2.16b), Gulf Fritillary (Fig. 2.16c), Queen Butterfly (Fig. 2.16d), and Buckeye Butterfly (Fig. 2.16e). The in-vivo experimental measurements were performed placing them carefully and fixing the insects onto a rigid surface, avoiding any wing damage and hence being able to perform the tests. The fixing method was suggested by an entomologist. The procedure followed was to first glue the insect legs to a metal post and with the help of a soft thread the main body was held by forming an "X" around it, as it is shown in Fig. 3.10.

Care was taken to allow the insect to move the wings freely and at the same time holding it strongly enough to perform the test. Each test lasted only a few seconds and then each insect was released from its fixings and set free. This procedure was the best option found to avoid the use of entomologic needles to pin the insect, a situation that without a doubt would have changed the wing natural movements. So, this method assured the minimum restriction to insects' natural movements and therefore it can be safely said that their wings were free to flap.

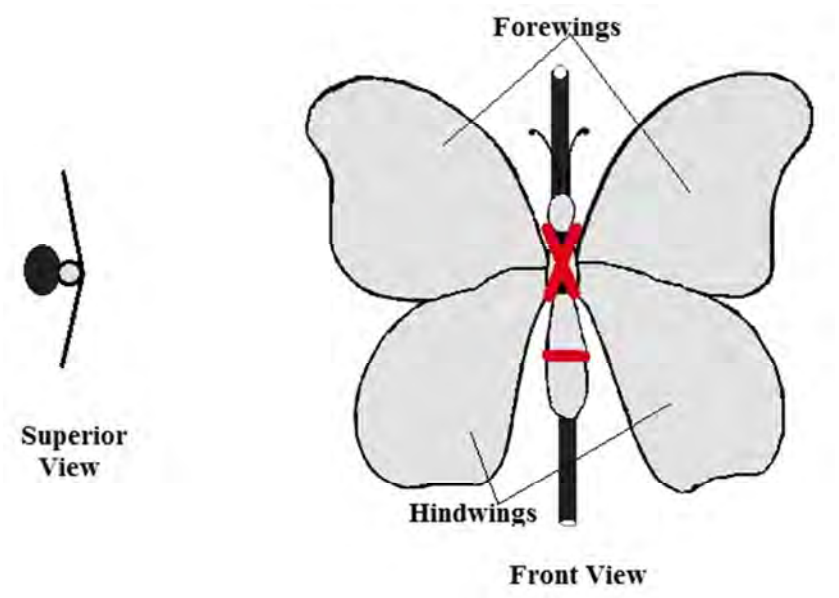


Fig. 3.10 Schematic view of the butterfly holding method.

The butterfly was fixed and placed in the optical experimental set up, of Fig. 3.11, which is similar to the optical set up shown in Fig. 3.7, but slightly adapted to work with the different testing subjects by changing optical components in the setup, a feature that will be described in the next lines. The out-of-plane optical set up uses the same Verdi laser, where the beam is divided with a beam splitter (BS) into an object and reference beams with a relation 70:30, respectively (approx. 2 W illuminates the wing with an illumination density

of 19.5 mW /cm$^2$ falling on the butterfly). The reference beam is launched into a single mode optical fibre (OF) using a 20x microscope objective (MO1), The object beam completely illuminates the insect wings surface using a 10X microscope objective (MO2), the backscattered light from the object passes through an aperture (A), and then is collected by the lens (L) located behind the aperture: these components are different from the optical setup described in section 3.2.

The object and the reference beams are combined at the CMOS sensor using a beam combiner (BC), with a field of view (FOV) (given by the lens-aperture combination) to observe the insect of 90 x 100 mm. The high speed camera (NAC GX-1) used has an image resolution of 800 x 800 pixels at 10 bits dynamic range, the camera parameters were adjusted automatically (according to the NAC-GX1 user's manual) since the speed recording was increased from 500 to 4000 fps due to the fastest movements presented by the insects in comparison with the one used in the experiment of section 3.2.

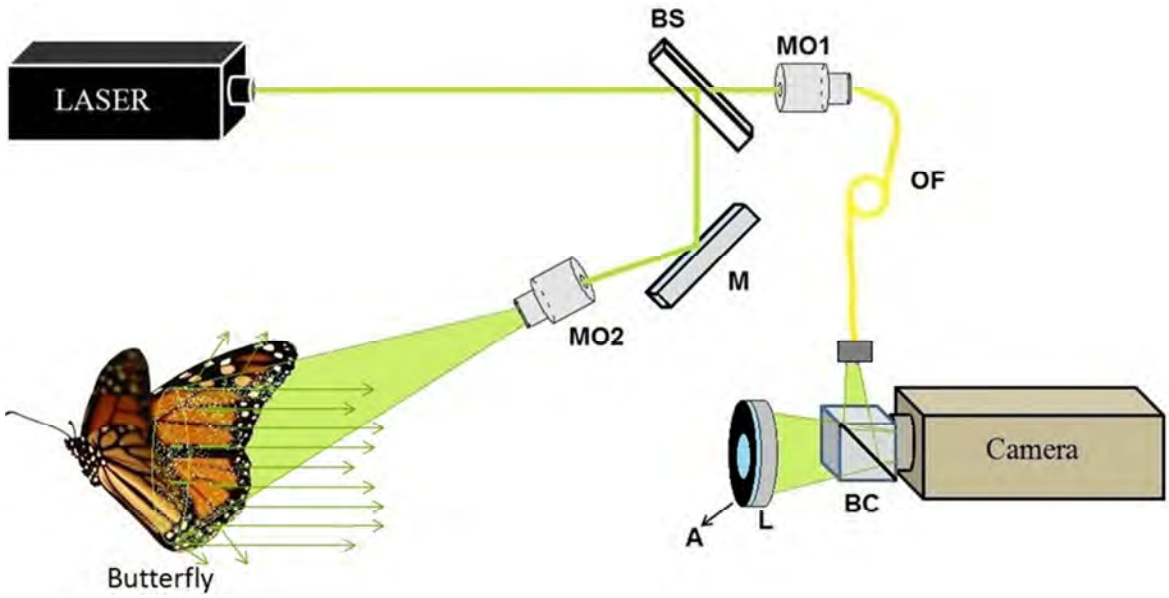


Fig. 3.11 DHI experimental set up with a high speed camera (CMOS technology).

The resultant wrapped phase maps obtained for each insect's wings are shown in Figs. 3.12 to 3.15. Each figure contains several images showing the wing motion behaviour of each butterfly during the experimental testing. These figures show the wing motion recorded at different moments for each butterfly. The best frame rate found to record all the images series was 4000 fps. During all the recording processes the electronic shutter of the CMOS camera was open for 102 µsec, significantly smaller than the exposure time of 250 µsec, a feature that avoids data averaging.

These figures represent particular states of each species during flapping at different moments, showing that there is not an equal motion pattern among the insect wings. The wrapped phase maps for the Mourning Cloak can be seen in Fig. 3.12, and each image represents different time instants during the test, the time lapse of the test is 0.2 secs. In these images it can be observed that any cyclic or regular movement is present considering the short time between the images. Fig.3.12 (a) and (b) show a different number of fringes and orientation, which is not the same as the rest of the images, this is a consequence of the short time between the images and the fast changes suffered by the wings. Fig. 3.12 (f) presents the larger number of fringes (right side) of all images implying a larger deformation in comparison with the other shown in Fig. 3.12 (c) and (d), while in Fig. 3.12 (e) it can be observed a larger deformation in the right side wings as compared to that in the left side wings. It may also be noticed that some sections have different deformations even for the same wing for all the images.

The wrapped phase maps from the images on Fig. 3.13 present more fringes on the left forewing and hindwing than the right side wings; this can be interpreted as a larger deformation during the 0.35 secs that the test lasts. The motion behaviour of the Agraulis Vanillae Incarnate is not a regular one and it is not even close to those observed in the butterflies of Figs. 3.12, 3.14 and 3.15. Fig. 3.13(a), (e) and (f) show more fringes than the rest of the images and in some sections a different deformation can be appreciated. If a comparison between images Fig. 3.13 (c) and (e) is made, it can be seen a larger deformation in the right side wings that the rest. And if we compare these images with those from the Nymphalis Antiopa (see Fig. 3.12) it is clear that they show a completely different behaviour of the insect's wings.

The images for the Danaus Gillipus Cramer shown in Fig. 3.14 present a really different number of fringes and an irregular orientation in them. The deformations affect more than a single section of the butterfly wings. Comparing the different images among them, the deformation is not even close to be regular or cyclic, since some wings present larger deformations in the right side as in Fig. 3.14 (a), while in (b) the four wings present a certain amount of deformation, and the next one shows a completely different behaviour from the previous ones. In the right hindwing it can be observed the way the deformation affects two sections of the same wing, while the rest are different, particularly in Fig. 3.14 (e) and (f). All these non-uniform changes are recorded during a lapse time of 0.2 secs.

The wrapped phase maps for the Precis Evarete Felder in Fig. 3.15 present some remarkable differences with respect to the other butterflies, such as the wings position that the butterfly adopted during the test, which lasted 0.17 secs. Fig. 3.15 (a), (c) and (e) present a fewer fringe number on the right side wings in comparison with the other three images, while observing the left side wing deformations the changes are not similar.

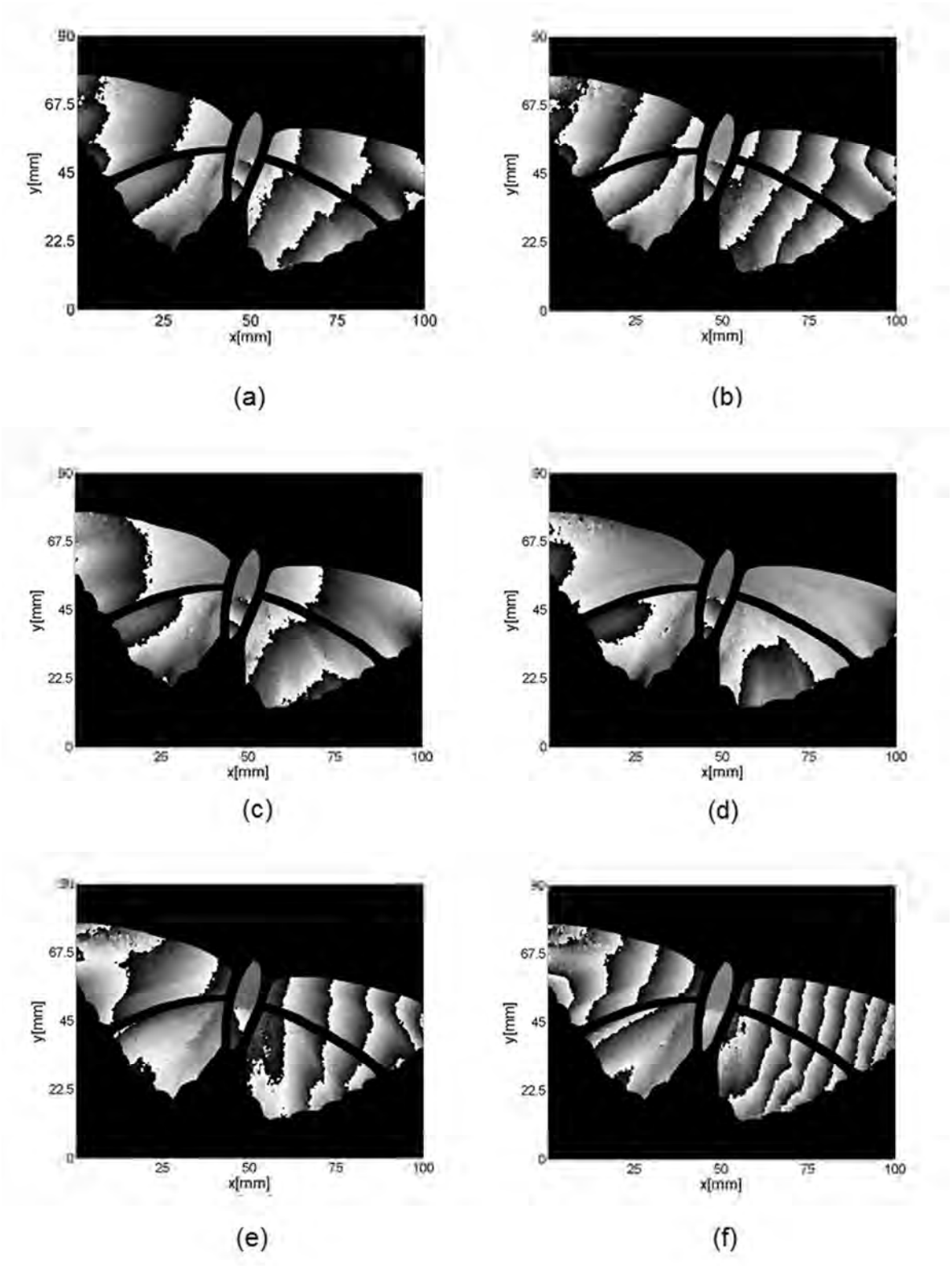


Fig. 3.12 Wing wrapped phase maps for *Nymphalis antiopa*, insect in Fig. 2.16(b).

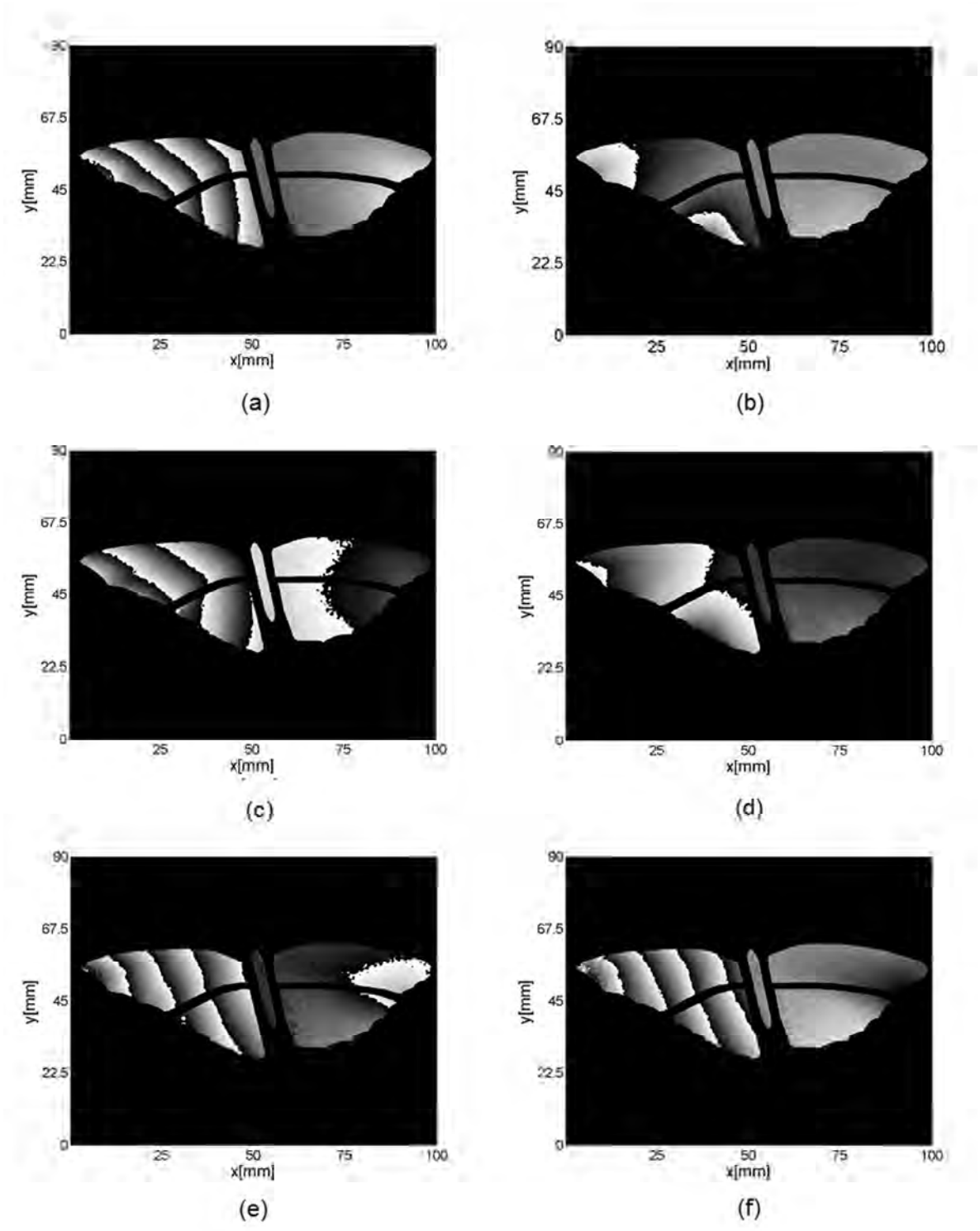


Fig. 3.13 Wing wrapped phase maps for *Agraulis Vanillae Incarnata*, insect in Fig. 2.16(c).

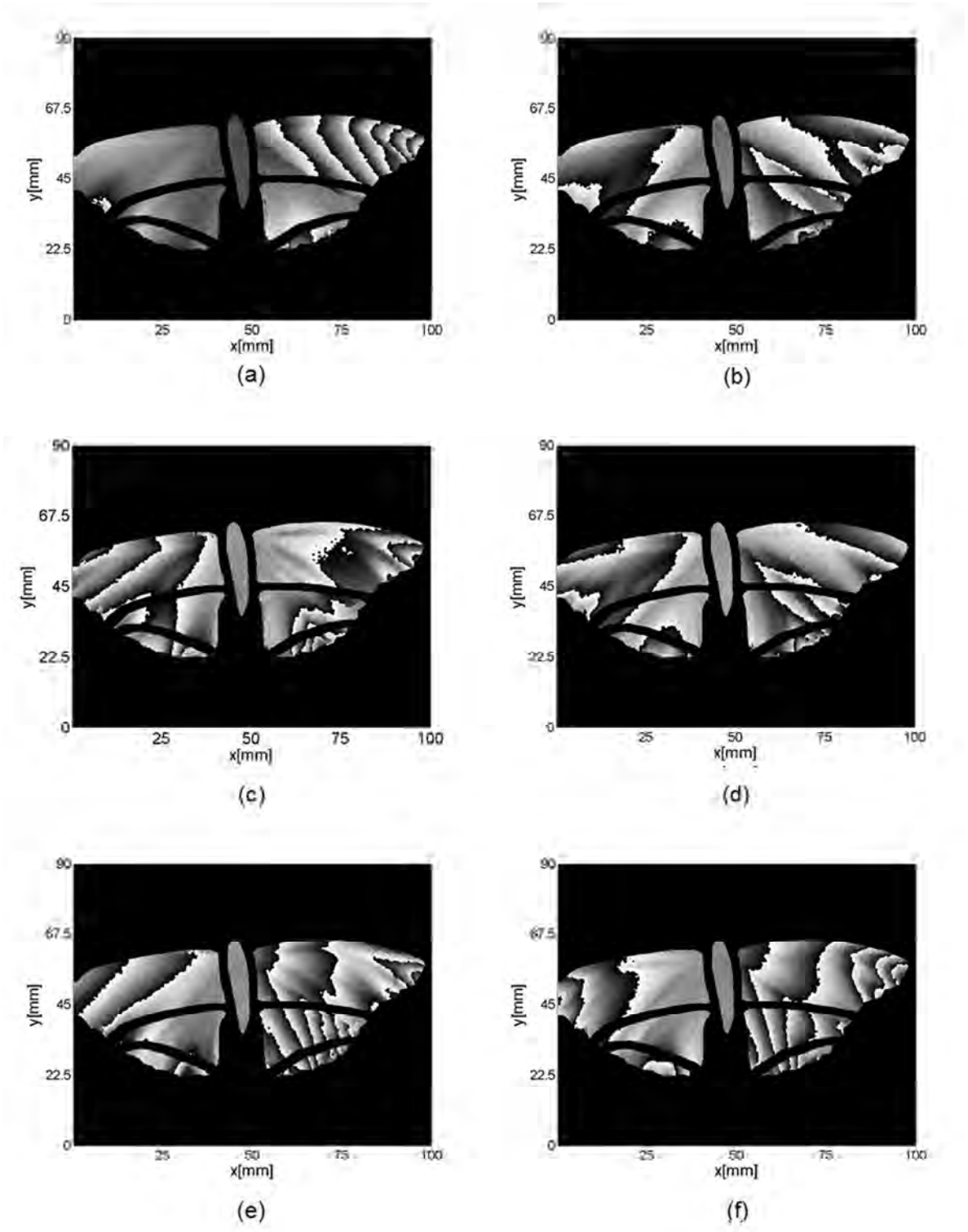


Fig. 3.14 Wing wrapped phase maps for *Danaus Gilippus Cramer*, insect in Fig. 2.16(d).

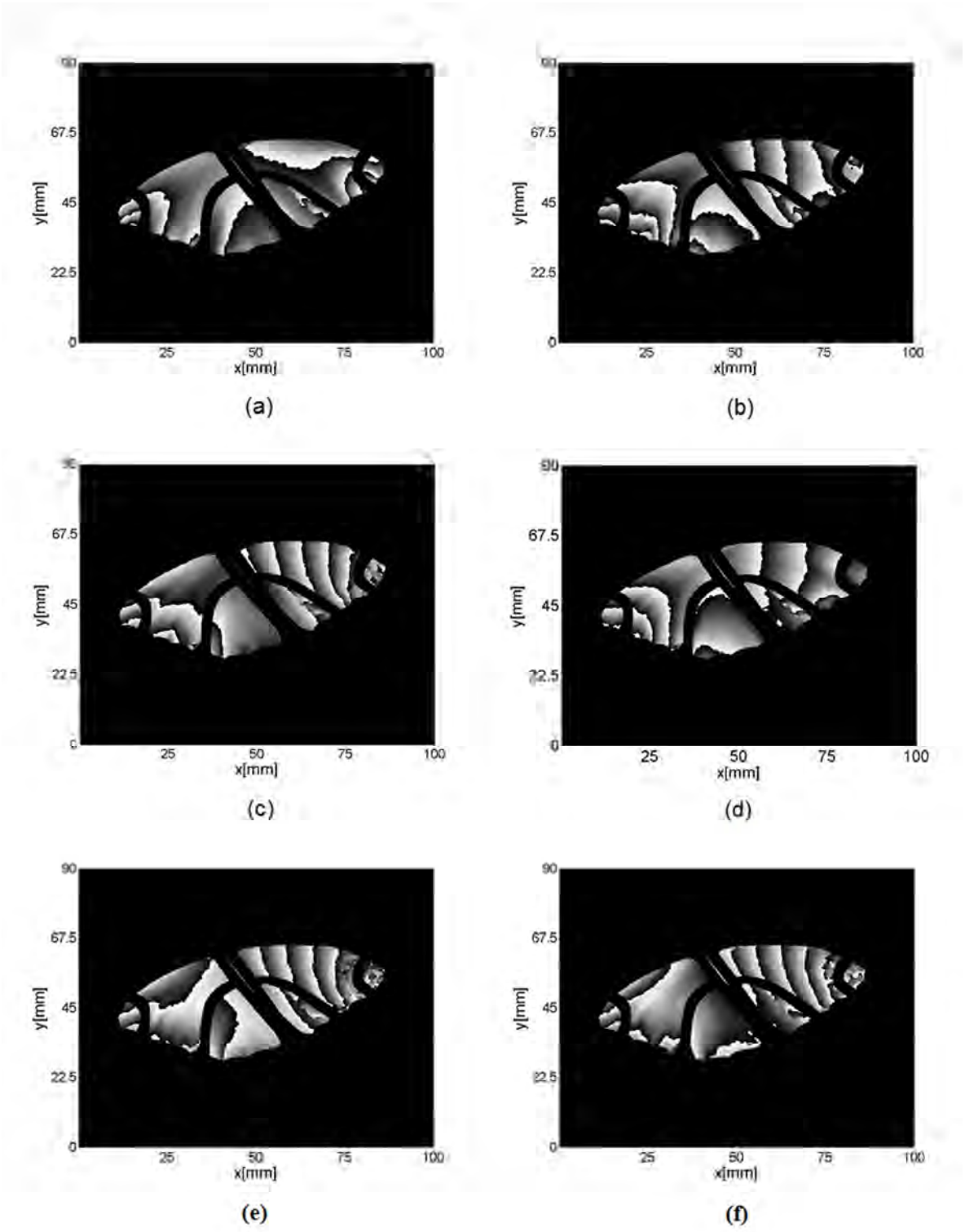


Fig. 3.15 Wing wrapped phase maps for *Precis Evarete Felder*, insect in Fig. 2.16(e).

The unwrapping procedure to recover the real displacements values from the wrapped phase maps shown in figures 3.12 to 3.15 is done using the same minimum cost match algorithm mentioned in section 3.2. The unwrapped phase maps for each butterfly are shown in figures 3.16 to 3.19 which present a colour bar indicating the maximum and minimum magnitude deformation value suffered by the wing during the motion.

In Fig, 3.16 the unwrapped phase maps for the Mourning Cloak show how different is the deformation suffered by each zone or part of the wings, e. g. observe images (a) to (d) where the left side wings present negative deformation values going from 0 to -0.4 µm, and the right wings present positive values from 0 to 0.4 µm, while images (e) and (f) show the opposite behaviour.

Comparing the Gulf Fritillary unwrapped phase maps of Fig. 3.17, the images (a) and (c) present negative values for the right side wings and the left side wings have values covering the range from -0.4 µm to 0.4 µm. Meanwhile the images (b) and (d) for the right side wings present positive values while the left ones cover the whole range of values.

Fig. 3.18 shows the unwrapped phase maps for the Queen Butterfly where it can be observed among the different images that the deformation over the upper and lower wings has no regular or cyclic change over the wings. The deformation values in the six images cover the range form -0.4 µm to 0.4 µm even in the same wing at different sections or zones of the wing.

The Buckeye Butterfly unwrapped phase maps are shown in Fig. 3.19, and it is easy to observe the range of deformation values for each wing where there are non uniform changes along the whole wing surfaces, provoking that certain sections present positive and negative values. In images (a) to (f) the upper wings present positive and negative deformation values but it has to be noticed that the lower wings show positive values only.

All of the above proves that each wing suffers deformations of different magnitude (positive and negative values) for different sections, even in the same wing. The latter can be interpreted as the way that each wing changes without a doubt in an independent way from each other.

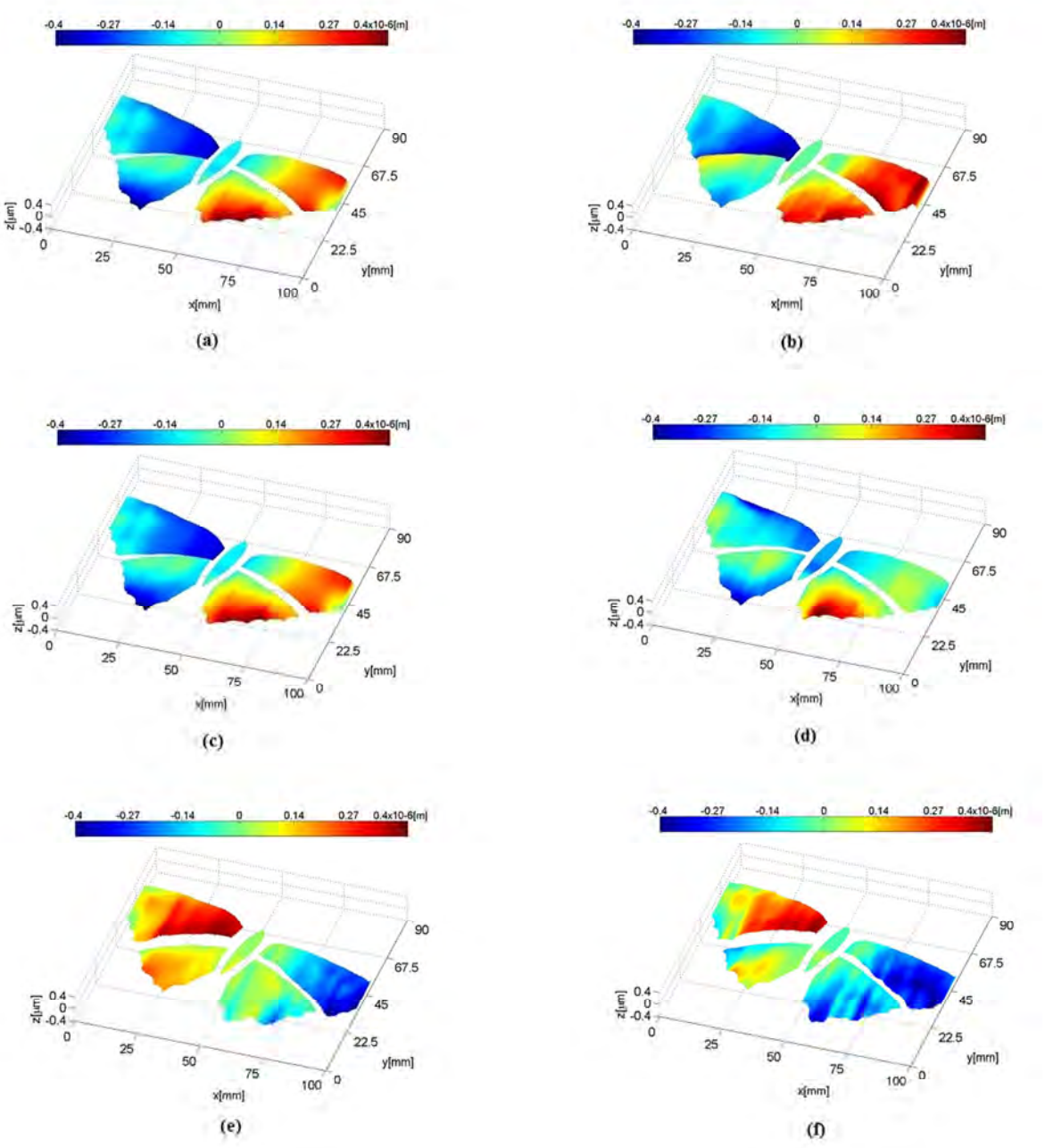


Fig. 3.16 Butterfly wings' surface deformation from DHI measuring experiments, showing different moments of the flapping for *Nymphalis Antiopa*, in Fig. 3.12.

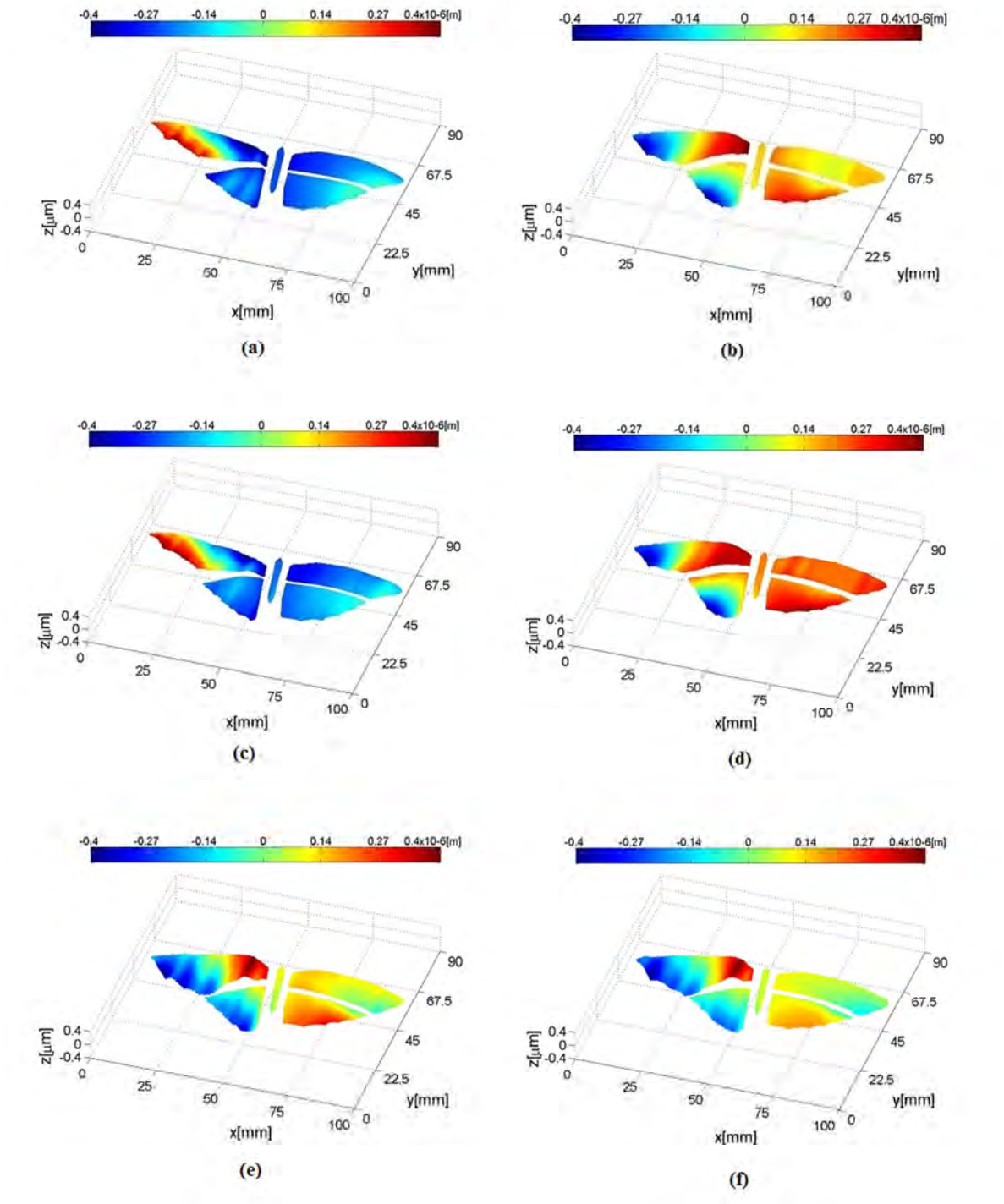


Fig. 3.17 Butterfly wings' surface deformation from DHI measuring experiments, showing different moments of the flapping for *Agraulis Vanillae Incarnata* in Fig. 3.13.

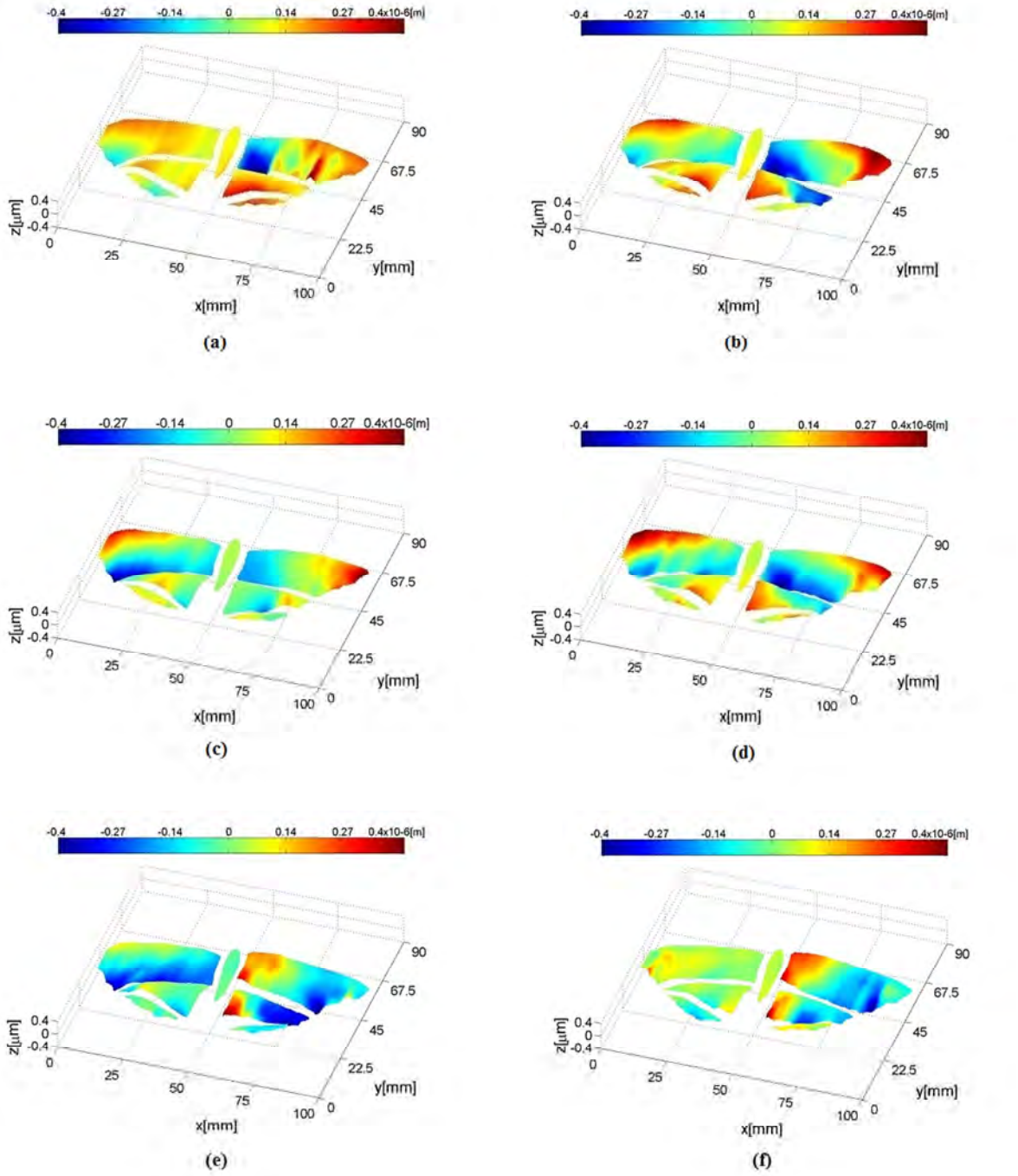


Fig. 3.18 Butterfly wings' surface deformation from DHI measuring experiments, showing different moments of the flapping for *Danaus Gilippus Cramer* in Fig. 3.14.

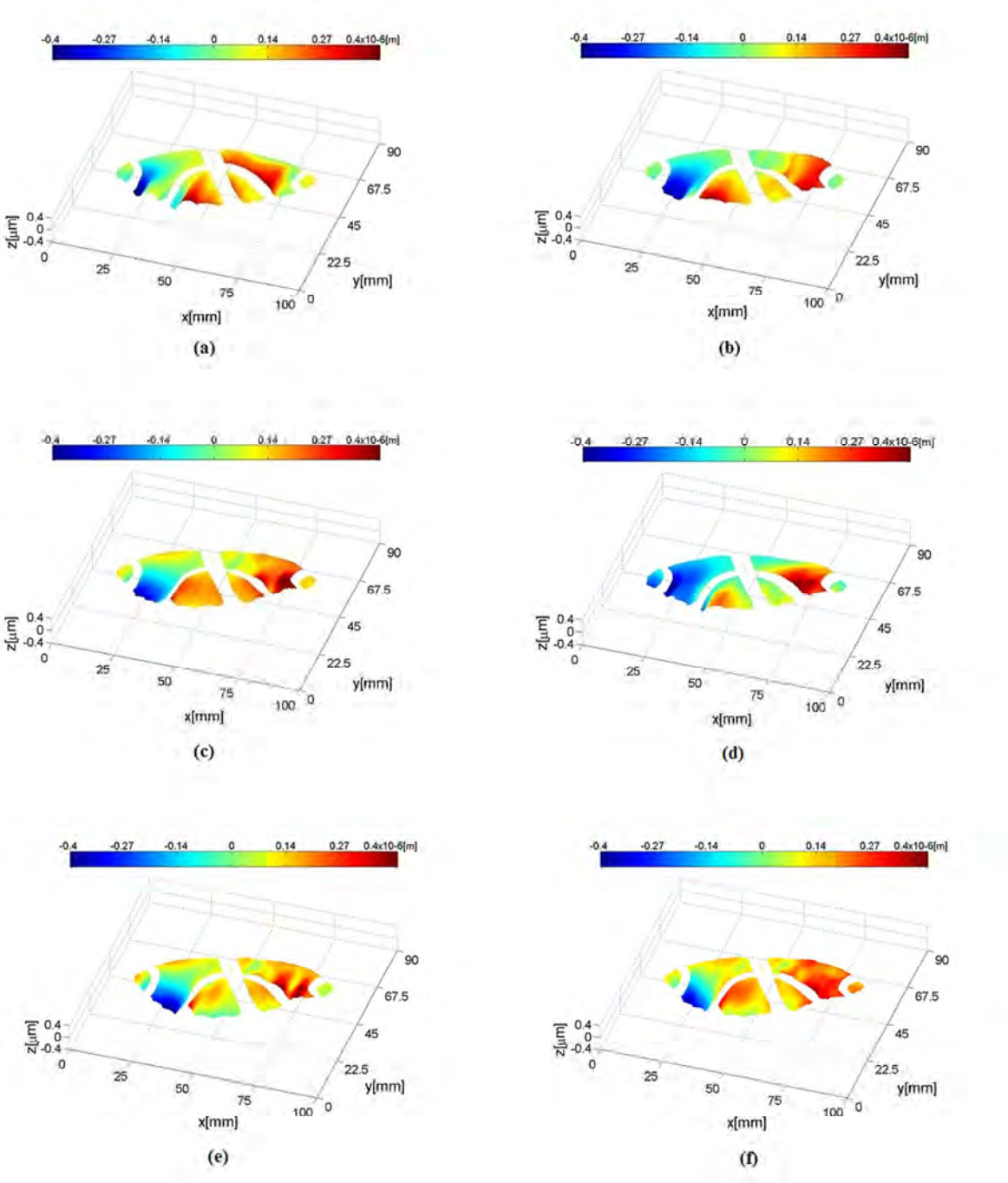


Fig. 3.19 Wing Butterfly wings' surface deformation from DHI measuring experiments, showing different moments of the flapping for for *Precis Evarete Felder* in Fig. 3.15.

A simple visual comparison from wrapped and unwrapped images of the butterfly's maps can be done, but to reinforce the hypothesis that no one moves equally or in the same magnitude, a close inspection of the movement is done. For this, a tracking was performed in the butterflies for each wing (forewings and hindwings) selecting randomly a line (starting at any point) and plotting its magnitude for each frame. This procedure is repeated for each butterfly.

Fig. 3.20 presents the result of the tracking displacement changes for each wing section among all the butterflies in a 50 frame series with a time interval of 250 μs between consecutive frames. Fig. 3.20 (a) represents displacement values among the butterflies' left forewing, while Fig. 3.20 (b) corresponds to the right forewing variations. The changes measured on the left and the right hindwings are plotted in Fig. 3.20(c) and 3.20(d), respectively. The plots coloured in black, blue, green and red represent wing changes for the Mourning Cloak, the Gulf Fritillary, the Queen Butterfly and the Buckeye Butterfly respectively.

From Fig. 3.20 it can be seen that for each specimen each wing has an independent movement. These figures also show the magnitude of the deformations presents in the insect's wings and how fast they can compensate these changes in a relatively short period of time (between consecutive images). These changes on butterflies wings' surface can be interpreted as a smooth variation in a macroscopic scale, but when it is recorded in high speed (micro seconds), it can be revealed that the wings' structure is adapted to fast changes in order to keep a relative steady flight.

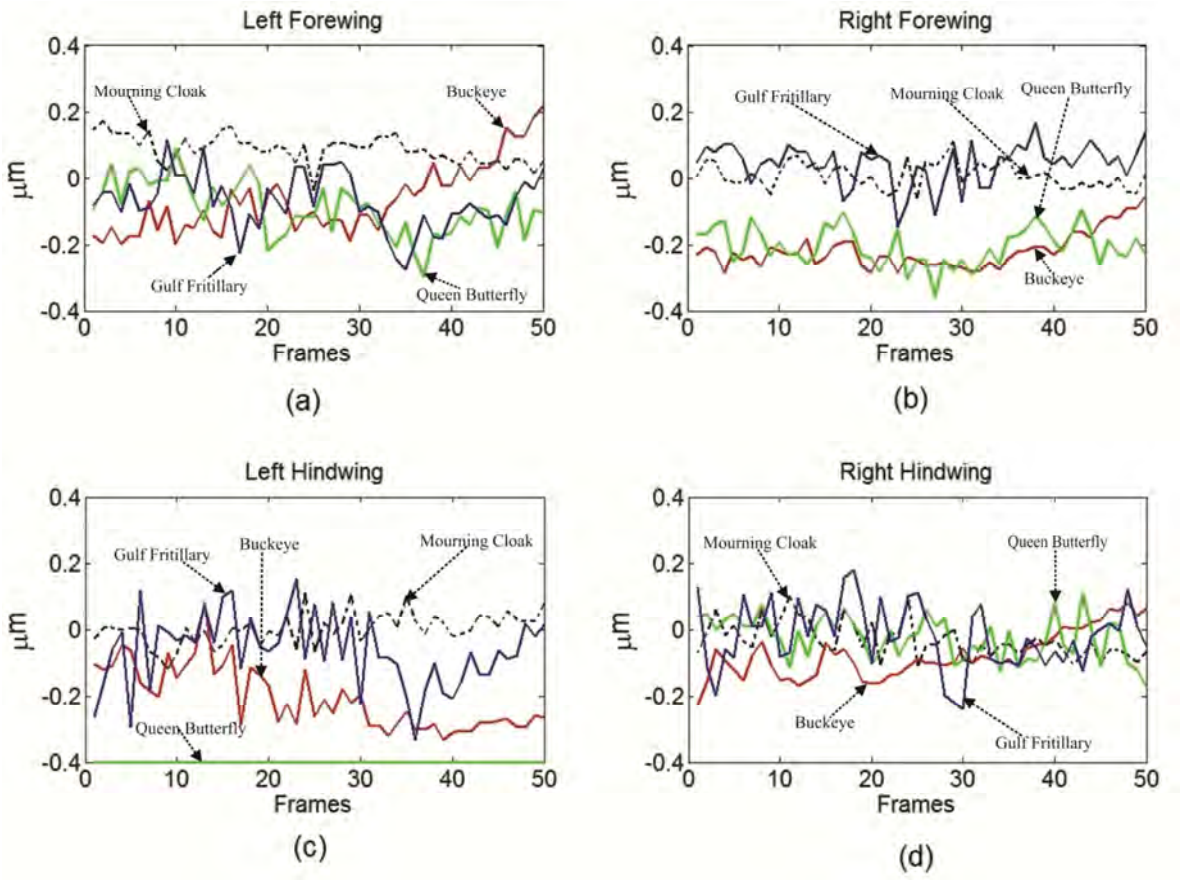


Fig. 3.20. A "first" data set (a), (b), (c) and (d). Butterfly wing displacement comparison between each wing section for each insect shown in Fig. 2.16(b)-(e).

A second comparison of the tracking displacement changes is performed on another set of images with the same number of frames and time between consecutive images. Fig 3.21 shows this second group of measurements where the curves are coloured in black, blue, green and red representing the same insects as in Fig. 3.20.

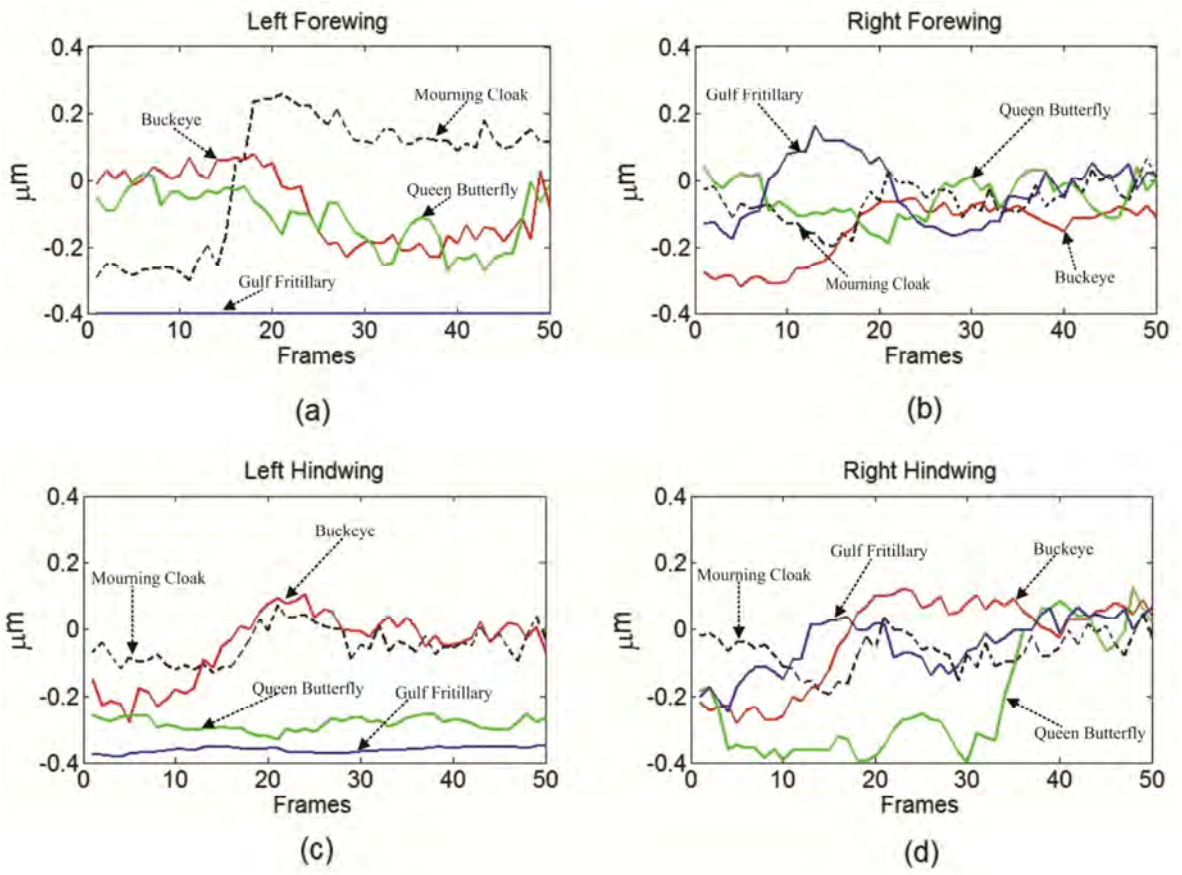


Fig.3.21. A “second” data set (a), (b), (c) and (d). Butterfly wing displacement comparison between each wing section for each corresponding insect shown in Fig. 2.16(b)-(e).

From Fig. 3.21(a) it can be noticed that for the Gulf Fritillary left forewing does not present any kind of movement, as in Fig. 3.20(c) the Queen Butterfly presents the same behaviour on the left hindwing. From Figs. 3.20 and 3.21 it can be noticed that wings can stay apparently in a static state while others keep on moving. Studying different butterflies with different sizes and characteristics can give us an idea of how fast an insect is able to change its position during flight in time intervals in the order of micro seconds (μs).

The discussion, the contributions and the general conclusions about the research work presented here are dealt within the next chapter.

# Chapter IV

## 4. Discussion and Conclusions

It can be safely stated that all the results presented here obtained using a non invasive optical method to study winged insect species with different characteristics and wing shapes, contribute to gain a better knowledge about what happens in the wings surface during flight. This represents a step ahead in insect flight behaviour understanding, and also pretends to add some information which may provide useful data that hopefully will contribute to improve the aero dynamical properties of human designed aircrafts, and particularly could be helpful to reproduce the complex characteristics involved in the insect flight motion. Also, it is a remarkable contribution the use of a non invasive optical technique to record the whole wing deformation, instead of researching on a single point. The work does not present results about what happens with the air flow provoked by the wing motion, instead it presents what is happening on the wing. The wing motion was not computer simulated or used with a robotic model which simulates the wing motion. Real insects were used to measure with high precision, deformations on the biological tissues that cover the wing's surface, looking for a better understanding about what happened during flight motion of winged insects, specifically 5 species of butterflies.

In recent years research on flying structures has been primarily focused in newer techniques like computer modelling, new pressure sensors, computational simulation, and flow visualization. As an alternative to these measurement techniques DHI has been applied to inspect biological samples, since it is a non contact/ non invasive/ non destructive measurement technique. DHI set up configurations can be modified to use the advantages of High Speed cameras, computers and imaging data processing. The latter keeps evolving

to improve the unwrapping methods to recover the data interferometrically encoded in the experimental results.

Chapter 3 showed how useful is DHI as an alternative option to record changes occurred on the whole wings' surface during flight, recovering real deformations (not simulated ones), and also allows to perform in vivo measurement, while a wing motion tracking is made on a single point selected randomly. DHI also showed that it can dealt with problems produced by biological tissues as the backscattering caused by dark sections on the wings (see Fig. 2.16), proving its sensitivity to record and measure transient and non repeatable events, like the wing flapping, where no single wing movement is equal or repeatable. This behaviour could be explained as a consequence of the wing's size, the form, the scale types and their alignment, the morphology and of course the flight conditions.

The five specimens chosen for this work are quite abundant in the local environment so there is not a chance to endanger their species. In all the experiments described for the insects in Fig. 2.16, the wing is considered as a whole unit, but further studies are needed in order to describe the effect of the scales present in a particular wing, which have an independent movement from each other. The experimental results obtained provide information that at this point no one else has reported in the internationally available literature using DHI, besides, any other optical technique used to perform measurements on insects.

The images from figures 3.8, 3.12, 3.13, 3.14 and 3.15 show how independent each wing is from each other, even from one section to another in the same wing, since each section responds in a completely different way. The wing responds in a really short period of time,

250 µsec between each recorded image. In these wrapped phase images it is possible to observe in the pattern some really marked changes in a particular section while in others apparently nothing seems to be happening.

Another fact that must be considered is the effect of the scales present on the wings, which under close observation have an independent movement from each other, having an important effect during flight motion. Sometimes the way butterfly aligns them provoke that the wing acts like a grating not having sign from the wing, because there is a weak backscattering light which avoids to perform the measurements.

These experiments and the conclusions obtained from the results are possible due to the fact that a high speed camera allowed to record non repeatable events, a feature not possible to observe with the naked eye or conventional cameras. There were many test/trials performed with only two sets of results presented in this thesis, both of them using the advantages of the high speed camera and its high resolution and sensitivity at 500 fps and 4000 fps. This allows to record images and data without the need of any extra data processing to extract the deformation map from the flapping (which was considered as a free wing motion).

The images for the different specimens in figures 3.8, 3.12, 3.13, 3.14 and 3.15., show that there are no uniform or symmetrical deformations between wings, remarking the fact that each butterfly presents a specific behaviour under the particular conditions mentioned above. Since the insect's wings have the capability and ability to adapt quickly to any changes in its flying motion, the same behaviour should not be expected each time that insects are flapping, since they try to adapt wings surface to compensate all the changes

suffered during flight. Also the same deformation pattern will never be presented by two specimens even if they come from the same species or had the same size, noticing this behaviour from the wrapped phase maps, each butterfly adopts a particular wing position during the flight motion and in consequence the deformation in some point is bigger than the one presented in other wing section even in the same butterfly.

The tracking line presented for the four butterflies plotted in figures 3.20 and 3.21 shows how different and quickly changes are present in the insect wings, this can be considered as a fast adaptation to quick changes since each image recorded represents a time difference of 250 µsec between them, and shows the motion followed by the wing during this short time lapse. Comparing the wings tracking from these figures, it can be observed that no single movement is equal in magnitude or lasts the same time. Also in Fig. 3.20(c) a remarkable behaviour is shown by the Queen Butterfly (green curve) on its left hindwing which is maintained without any movement while the other three wing sections actually have movement through the whole plot. This behaviour can be expected since the time lapse plotted for the 50 images series lasts 12.5 msec, short enough to present this kind of response.

Fig. 3.20 presents results for a “first” series of 50 frames, and Fig. 3.21 presents another plot for a “second” different series of images that produce two remarkable highlights in left forewing motion behaviour: In Fig. 3.21 (a), the Mourning Cloak (black curve) presents an ascending movement which can be interpreted as a quick movement of the butterfly wing increasing the motion velocity, or as the movement to gain impulse in the flight. Also in this figure the Gulf Fritillary show no movement in the left forewing as in Fig. 3.20 (c) the

Queen Butterfly did. This behaviour shows how adaptive is each insect wing, and at some point it can be interpreted as if that wing is probably compensating the violent movement performed by the other three wing sections. From these comparisons between line tracking plots, it can be concluded that if several line tracking plots are processed for different images series, they will present very different results for each image series.

The research work conducted shows that Digital Holographic Interferometry is an alternative tool to flow visualization, computer modelling, micro robotics model and all the computer insect wing simulation, even to other traditional measurement techniques, providing a non destructive option to measure non repeatable events described by the whole wing surface. Indeed, all the results presented here are showing the phenomenon of the insects' wing deformation suffered, and not its mechanicals characteristics, leaving them for future research work.

Also there is a strong belief that future study and research on insect wing flapping will render useful data that will no doubt contribute to better understand the aero dynamical properties of human designed aircrafts and improved their performances based on the insects' wing motion performances, and finally do a reliable copy of them.

Since this is only a small part of a huge developing work involving researchers, engineers, entomologists and many industries in this research area, the future work that can be derived from the one reported here, will quantify and measure mechanical properties such as stiffness and elasticity. And also, the use of trained insects to perform a 100 % free wing motion that could provide new data from the wings.

The results obtained and presented from this research work have a significant relevance, and they were published in two recognized scientific journals: the research work was awarded with the front covers of the online journal Optics Express® and The Virtual Journal of Biomedical Optics®, both of them from the Optical Society of America (OSA)®.

# Chapter V

## 5.1 References

[1] Armstrong, R. H. 1990, “Photographing insects in flight,” *American Entomologist*, Vol. 36, No. 3.

[2] Pringle, J. W. *S.*, **Insect Flight**, (Cambridge University Press, 1957).

[3]R. Jones and C. Wykes, **Holographic and Speckle Interferometry** (Cambridge Univ. Press, 1989).

[4] K. J. Gasvik, **Optical Metrology** (John Wiley & Sons, Ltd., 2002).

[5] R. K. Erf, **Holographic Nondestructive Testing** (Academic Press Inc., 1974).

[6]C. M. Vest, **Holographic Interferometry** (John Wiley & Sons, 1979).

[7]P. K. Rastogi, **Digital Speckle Pattern Interferometry and Related Techniques** (John Wiley & Sons, Ltd., 2001).

[8] Thomas Kreis, **Holographic and speckle interferometry** (Akademie Verlag, 1996).

[9] Noe Alcalá Ochoa, Fernando Mendoza Santoyo, Carlos Pérez López, and Bernardino Barrientos, "Multiplicative Electronic Speckle-Pattern Interferometry Fringes," Appl. Opt. 39, 5138-5141 (2000).

[10] Staffan Schedin, Giancarlo Pedrini, and Hans J. Tiziani, “Pulsed digital holography for deformation measurements on biological tissue,” Appl. Opt. 39, 2853–2857 (2000).

[11] D. L. Grodnitsky, **Form and Function of Insect Wings** (John Hopkins University, 1999).

[12] R. Dudley, **The biomedical of insect flight** (Princeton University Press, 2000).

[13] Sanjay P. Sane, “The aerodynamics of insect flight,” J. Exp. Biol. 206, 4191- 4208 (2003).

[14] C. P. Ellington, “The novel aerodynamics of insect flight: applications to micro-air vehicles”, J. Exp. Biol. 202, 3439-3448 (1999).

[15] T. L. Hedrick, J. R. Usherwood, and A. A. Biewener, “Wing inertia and whole-body acceleration: an analysis of instantaneous aerodynamic force production in cockatiels (Nymphicus hollandicus) flying across a range of speeds,” J. Exp. Biol. 207, 1689-1702 (2004).

[16] J. R. Usherwood, and C. P. Ellington, “I. Model hawkmoth wings,” J. Exp. Biol. 205, 1547-1564 (2002).

[17] S. J. Steppan, “Flexural stiffness patterns of butterfly wings (Papilionoidea),” J. Res. on the Lepidoptera, 35, 61-67 (1996).

[18] S.A. Combes, and T. L. Daniel, “Flexural stiffness in insect wings I. Scaling and the influence of wing venation,” J. Exp. Biol. 206, 2979-2987 (2003).

[19] J. R. Usherwood, and C. P. Ellington, “The aerodynamics of revolving wings II: Propeller force coefficients from mayfly to quail,” J. Exp. Biol. 205, 1565–1576 (2002).

[20] S. Sudo, K. Tsuyuki and K. Kanno,“Wings characteristics and flapping behavior of flying Insects,” JSEM 45, 550-555 (2005).

[21] R. B. Srygley and A. L. R. Thomas, “Unconventional lift-generating mechanisms in free-flying butterflies,” Nature 420, 660-664 (2002).

[22] A. L. R. Thomas, G. K. Taylor, R. B. Srygley, R. L. Nudds, and R. J. Bomphrey, “Dragonfly flight: free-flight tethered flow visualizations reveal a diverse array of unsteady lift-generating mechanisms, controlled primarily via angle of attack,” J. Exp. Biol. 207, 4299-4323 (2004).

[23] Hoell, H.V., Doyen, J.T. & Purcell, A.H., **Introduction to Insect Biology and Diversity** (Oxford University Press, 1998)

[24] Gullan, P.J.; P.S. Cranston, **The Insects: An Outline of Entomology,** (Oxford: Blackwell Publishing, 2005)

[25] M. Dickinson, "Solving the mystery of insect flight," Scientific American, June, 34-41 (June 2001).

[26] J. Yan, R. J. Wood, S. Avadhanula, M. Sitti, and R. S. Fearing, "Towards flapping wing control for a micromechanical flying insect," in Proceedings of IEEE Conference Robotics and Automation Vol. 4, pp. 3901-3908, Seoul Korea, May 21-26 (2001)..

[27] S. Avadhanula, R. J. Wood, E. Steltz, J. Yan, and R. S. Fearing, "Lift force improvements for the micromechanical flying insect," in Proceedings of IEEE International Conference on Intelligent Robots and Systems Vol. 2, Las Vegas, Nevada, pp. 1350–1356 (2003).

[28] L. D. Wallace, N. J. Lawson, A. R. Harvey, J. D.C. Jones, and A. J. Moore, "High Speed photogrametry for measuring the kinematics of insect wings," Appl. Opt., 45, 4165-4173 (2006).

[29] Carlos Pérez-López, Manuel H. De la Torre-Ibarra, and Fernando Mendoza Santoyo, "Very high speed cw digital holographic interferometry," Opt. Exp. 14, 9709- 9715 (2006).

[30] S. Sunada, D. Song, X. Meng, H. Wang, L. Zeng, and K. Kawachi, "Optical measurement of the deformation, motion and generated force of the wings of a moth, Mythima separate (Walker)," JSME Int. J. Ser. B 45, 836–842 (2002).

[31] I. R. Hooper, P. Vukusic, and R. J. Wootton, "Detailed optical study of the transparent wing membranes of the dragonfly.

[32] Malacara, Daniel, **Optica Basica,** (Fondo de Cultura Economica, 2006).

[33] Hetch, **Optics**, (Addison Wesley, 2001).

[34] De la Torre Ibarra, Manuel, 3D digital holographic interferometry and spectral optical coherence tomography for the measurement of strain in metallic objects and phase in biological tissues, Ph. D. Thesis (2006).

[35] Mitsuo Takeda, Hideki Ina and Seiji Kobayashi,"Fourier-transform method of fringe-pattern analysis for computer-based topography and interferometry," J. Opt. Soc. Am. 72, 156 - 160 (1982).

[36] D. Malacara, M. Servin and Z. Malacara, **Interferogram Analysis for Optical Testing** (Marcel Decker, 1998).

[37] Ichirou Yamaguchi, Speckle Displacement and Decorrelation in the Diffraction and Image Fields for Small Object Deformation, Optica Acta:International Journal of Optics, 28:10, 1359-1376 (1981).

[38] Yamaguchi, I., Simplified laser-speckle strain gauge, Optical Engineering, Vol. 21, pp. 436-440. May-June 1982.

[39] Yamaguchi, I., Fringe formation in speckle photography, J. Opt. Soc. A 81, Vol. 1, No. 1, (1984).

[40] De la Torre Ibarra, Manuel, Aplicación de la Interferometría de Patrones de Moteado y la Holografía Digital al Estudio de Deformaciones en 3D en Piezas Metálicas, Tesis de Maestria (2003).

[41] D.J. Borror, .M. De Long, A. Triplehorn A. and J Norman, Introduction to the study of insects, (Thomson Brooks/ Cole, 2005).

[42] J. G. Kingsolver and MAR. Koehl, "Selective factors in the evolution of insects kings," Annu. Rev.. Entomol. 39, 425–451 (1994).

[43] S. Sudo and K. Tsuyuki, “Wing morphology of some insects,” JSME International Journal Series C, 43(4):895–900 (2000).

[44] R. F.Chapman, The Insects: Structure and Function, (Hodder and Stoughton, 1982).

[45] Fang Y., S. Gang, Q. Cong, G Chen and L. Ren, Effects of methanol on wettability of the nonsmooth surface on butterfly wing. Journal of Bionic Engineering 5 (2), 127-133 (2008).

[46] S. A. Combes and T. L. Daniel, Flexural stiffness in insect wings II. Spatial distribution and dynamics wing bending. J. of Exp. Biol. 206, 2989-2997 (2003).

[47] R.J. Wootton, Functional morphology of insect wings. Annual Review Entomology. 37. 113-140 (1992).

[48] H. F. Nijhout, Elements of Butterfly Wing Patterns, J. Exp. Zoo., 291, 213– 225, (2001).

[49] J.E. De la Maza, **Mariposas Mexicanas: Guía para su colecta y determinación** (Fondo de Cultura Mexicana, 1987).

[50] C. R. Beultelspacher, **Mariposas diurnas del Valle de México**, (Ediciones Científicas L.P.M.M., 1980).

[51] H. L. Lewis, **Butterflies of the World** (Harrison House, 1987).

[52] Cech, R. and Tudor, G., **Butterflies of the East Coast,** (Princeton University Press, 2005).

[53] Giancarlo Pedrini, Wolfgang Osten and Mikhail E.Gusev, "High-speed digital holographic interferometry for vibration measurement," Appl. Opt. 45, 3456 - 3462 (2006).

[54] Staffan Schedin, Giancarlo Pedrini, Hans J. Tiziani, and Fernando Mendoza Santoyo, "Simultaneous three-dimensional dynamic deformation measurements with pulsed digital holography," Appl. Opt. 38, 7056-7062 (1999).

[55] Manuel De la Torre-Ibarra, Fernando Mendoza-Santoyo, Carlos Pérez-López, and Tonatiuh Saucedo-A., "Detection of surface strain by three-dimensional digital holography," Appl. Opt. 44, 27-31 (2005).

[56] Manuel De la Torre-Ibarra, Fernando Mendoza Santoyo, Carlos Perez-Lopez, Tonatiuh Saucedo A. and Daniel D. Aguayo, “Surface strain distribution on thin metallic plates using 3-D digital holographic interferometry,” Optical Engineering 45 (10), (2006).

[57] A. Fernández, A. J. Moore, C. Pérez-López, A. F. Doval, and J. Blanco-García, "Study of transient deformations with pulsed TV holography: application to crack detection," Appl. Opt. 36, 2058-2065 (1997).

[58] Nandigana Krishna Mohan, Angelica Andersson, Mikael Sjödahl, and Nils-Erik Molin, “Optical configuration for TV holography measurement of in-plane and out-of-plane deformations,” Appl. Opt. 39, 573-577 (2000).

[59] Jose L. Marroquin, Maximino Tapia, Ramon Rodriguez-Vera, and Manuel Servin, "Parallel algorithms for phase unwrapping based on Markov random field models," J. Opt. Soc. Am. A 12, 2578 - 2585 (1995).

[60] Manuel Servin, Jose Luis Marroquin, Daniel Malacara, and Francisco Javier Cuevas, "Phase Unwrapping with a Regularized Phase-Tracking System," Appl. Opt. 37, 1917-1923 (1998)

[61] D. C. Ghiglia and L. A. Romero, “Robust two-dimensional weighted and unweighted phase unwrapping that uses fast transforms and iterative methods,” J. Opt. Soc. Am. A 11,107–117 (1994).

[62]. J. M. Huntley, “Noise-immune phase unwrapping algorithm,” Appl. Opt. 28, 3268–3270 (1989).

[63] Daniel D. Aguayo, Fernando Mendoza Santoyo, Manuel H. De la Torre-I, Cristian Caloca-Mendez, “Insect Wing Displacement Measurement Using Digital Holography”, RIAO/OPTILAS 2007: 6th Ibero-American Conference on Optics (RIAO); 9th Latin-American Meeting on Optics, Lasers and Applications (OPTILAS), Campinas, São Paulo (Brazil), 21–26 October 2007

[64] Daniel D. Aguayo, Fernando Mendoza Santoyo, Manuel H. De la Torre-I, Manuel D. Salas-Araiza, Cristian Caloca-Mendez and David Asael Gutierrez Hernandez, “Insect wing deformation measurements using high speed digital holographic interferometry”, Opt. Exp.,18, 5661-5667(2010)

## 5.2 Figure List

# Appendix A

# A.1 Wings Sections

This section describes in a brief way all butterfly wings sections, these terms are cited in chapter 2 and are explained in the lines below.

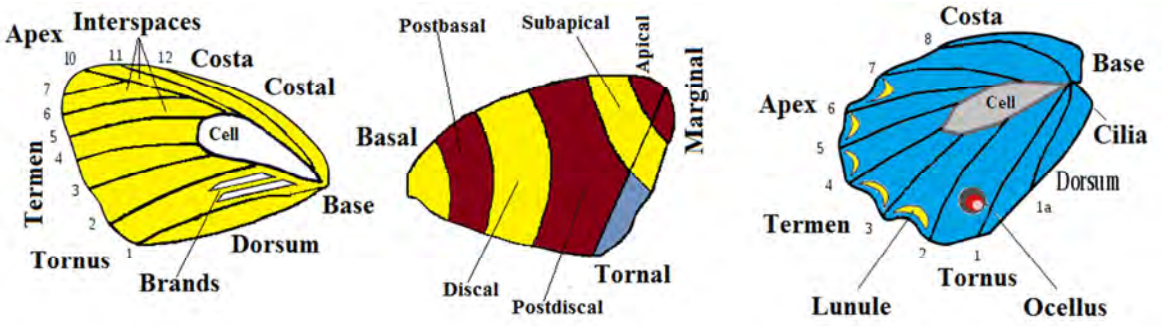


Fig.A.1 Butterfly wing parts

- **Admarginal**: Along the wing margin.
- **Anal angle**: The posterior corner of the wing (same as tornus).
- **Androconium or androconia**: Specialised microscopic scales on the wings of male butterflies, believed to be scent scales for attracting the female
- **Annular**: Ring-shaped.
- **Apex / Apical area**: The anterior corner of the wing.
- **Areola**: A small subdivision at the base of the wing cell, or a small "window" on the upper side of a wing scale.
- **Base / Basal area of wing**: Region close to the point of attachment to the thorax.
- **Brand**: Raised area on the wing surface, circular, ovate, or elongated, which is covered with special scent scales or androconia, found in males of some species (also called sex mark).

- **Catenulate**: Markings consisting of rings connected together like a chain.
- **Cell**: The central area surrounded by veins. It can be closed by veins or open.

  -The vein forming the boundary of the cell along the costal margin is known as the subcostal vein.

  -The vein forming the lower boundary towards the dorsum is called the median vein.

  -In the case of butterflies, the cell is closed by a vein connecting the origins of veins 6 to 4 along the top of the cell which is known as discocellular vein.
- **Cilia**: Fine hairs along the edges of the wing.
- **Costa / Costal area**: The leading edge of the wing.
- **Crenulate**: Term used to describe the outer edge of the wing, when it is scallopped, i.e., convex at the end of each vein, and, concave in between.
- **Dentate**: As for crenulate but with the projections at the end of each wing being toothlike.
- **Disc / Discal area**: The central band passing through the cell.
- **Dorsum / Dorsal area**: Referring to the trailing edge or hind-margin of the wing, extending from the base to the tornus. Dorsal alternately, also refers to the back, i.e. the upper part of the body, from above.
- **Fascia (plural Fasciae)**: Refers to a colour pattern with a broad band.
- **Eyespot or Ocelli**: Spots resembling mammalian eyes. Can

also be used to refer to simple eyes.

- **Interspace**: The region between adjacent veins.
- **Irrorated or írroration**: Old term used usually to indicate a sprinkling of scales interspersed among scales typically of a different colour.
- **Lunule**: Crescent marks usually found along the margin.
- **Nervure**: Older term for vein. Adnervural is used to describe for instance lines running adjacent and alongside the veins.
- **Stigma (plural Stigmata)**: Prominent cells on the forewings of some moths. Their size, shape and colour can be useful in identifying some species.
- **Strigae**: Refer patterns with thin lines.
- **Terminal and marginal**: Along the margin.
- **Termen**: The edge of the wing most distant from the body.
- **Tornus / Tornal area**: The posterior corner of the wing.
- **Vein**: Hollow structures formed from the coupling of the upper and lower walls of the wing. They provide both rigidity and flexibility to the wing.

# Appendix B

# B.1. Taxonomy of Pterourus Multicaudata

Fig. B.1 *Pterourus Multicaudata* known as Eastern Tiger Swallowtail.

- **Domain:** Eukaryota
- **Kingdom:** Animalia
- **Subkingdom:** Bilateria
- **Branch:** Protostomia
- **Infrakingdom:** Ecdysozoa
- **Superphylum:** Panarthropoda
- **Phylum:** Arthropoda
- **Subphylum:** Mandibulata
- **Infraphylum:** Atelocerata
- **Superclass:** Panhexapoda
- **Epiclass:** Hexapoda
- **Class:** Insecta
- **Subclass:** Dicondylia
- **Infraclass:** Pterygota
- **Cohort:** Myoglossata
- **Order:** Lepidoptera
- **Infraorder:** Heteroneura
- **Family:** Papilionidae
- **Subfamily:** Papilioninae
- **Genus:** Papilio
- **Specific name:** glaucus
- **Scientific name:** Pterourus Multicaudat

## B.2 Taxonomy of Nymphalis Antiopa

Fig. B.2 *Nymphalis Antiopa* known as Mourning Cloak.

- **Domain:** Eukaryotas
- **Kingdom:** Animalia
- **Subkingdom:** Bilateria
- **Branch:** Protostomia
- **Infrakingdom:** Ecdysozoa
- **Superphylum:** Panarthropoda
- **Phylum:** Arthropoda
- **Subphylum:** Mandibulata
- **Infraphylum:** Atelocerata
- **Superclass:** Panhexapoda
- **Epiclass:** Hexapoda.
- **Class:** Insecta.
- **Subclass:** Dicondylia
- **Infraclass:** Pterygota
- **Cohort:** Myoglossata
- **Superorder:** Amphiesmenoptera
- **Order:** Lepidoptera.
- **Infraorder:** Heteroneura.
- **Family:** Nymphalidae.
- **Subfamily:** Nymphalinae.
- **Genus:** Nymphalis
- **Specific name:** antiopa.
- **Scientific name:** Nymphalis antiopa

## B.3 Taxonomy of Agraulis Vanillae Incarnata

Fig. B.3 *Agraulis Vanillae Incarnata* known as Gulf fritillary.

- **Domain:** Eukaryota
- **Kingdom:** Animalia
- **Subkingdom:** Bilateria
- **Branch:** Protostomia
- **Infrakingdom:** Ecdysozoa
- **Superphylum:** Panarthropoda
- **Phylum:** Arthropoda
- **Subphylum:** Mandibulata
- **Infraphylum:** Atelocerata
- **Superclass:** Panhexapoda
- **Epiclass:** Hexapoda
- **Class:** Insecta
- **Subclass:** Dicondylia
- **Infraclass:** Pterygota
- **Cohort:** Myoglossata
- **Superorder:** Amphiesmenoptera
- **Order:** Lepidoptera
- **Infraorder:** Heteroneura
- **Family:** Nymphalidae
- **Subfamily:** Heliconiinae
- **Genus:** Agraulis
- **Specific name:** vanillae
- **Subspecies:** incarnata
- **Scientific name:** Agraulis vanillae incarnata

## B.4 Taxonomy of Danaus Gilippus Cramer

Fig. B. 4 *Danaus Gillipus Cramer* known as Queen Butterfly.

- **Domain:** Eukaryota
- **Kingdom:** Animalia
- **Subkingdom:** Bilateria
- **Branch:** Protostomia
- **Infrakingdom:** Ecdysozoa
- **Superphylum:** Panarthropoda
- **Phylum:** Arthropoda
- **Subphylum:** Mandibulata
- **Infraphylum:** Atelocerata
- **Superclass:** Panhexapoda
- **Epiclass:** Hexapoda
- **Class:** Insecta
- **Subclass:** Dicondylia
- **Infraclass:** Pterygota
- **Cohort:** Myoglossata
- **Superorder:** Amphiesmenoptera
- **Order:** Lepidoptera
- **Infraorder:** Heteroneura
- **Family:** Nymphalidae
- **Group:** Nymphalinina
- **Subfamily:** Danainae
- **Genus:** Danaus
- **Specific name:** gilippus
- **Scientific name:** Danaus gilippus Cramer

## B.5 Taxonomy of Precis Evarete Felder

Fig. B.5 *Precis Evarete Felder* known as Buckeye butterfly.

- **Domain:** Eukaryota
- **Kingdom:** Animalia
- **Subkingdom:** Bilateria
- **Branch:** Protostomia
- **Infrakingdom:** Ecdysozoa
- **Superphylum:** Panarthropoda
- **Phylum:** Arthropoda
- **Subphylum:** Mandibulata
- **Infraphylum:** Atelocerata
- **Superclass:** Panhexapoda
- **Epiclass:** Hexapoda
- **Class:** Insecta
- **Subclass:** Dicondylia
- **Infraclass:** Pterygota
- **Cohort:** Myoglossata
- **Superorder:** Amphiesmenoptera
- **Order:** Lepidoptera
- **Infraorder:** Heteroneura
- **Family:** Lycaenidae
- **Genus:** Precis
- **Specific name:** evarete
- **Scientific name:** Precis evarete Felder